

A LARGE SYSTEMATIC SEARCH FOR RECOILING AND CLOSE SUPERMASSIVE BINARY BLACK HOLES

MICHAEL ERACLEOUS^{1,2}, TODD A. BOROSON³, JULES P. HALPERN⁴, & JIA LIU⁴

Submitted to the Astrophysical Journal Supplements on 10 June 2011

ABSTRACT

We have carried out a systematic search for *close* supermassive black hole binaries (with sub-parsec separations) among $z \lesssim 0.7$ quasars observed spectroscopically in the Sloan Digital Sky Survey. Such binaries are predicted by models of supermassive black hole and host galaxy co-evolution, therefore their census and population properties constitute an important test of these models. Our working hypothesis is that one of the two black holes accretes at a much higher rate than the other and carries with it the only broad-emission line region of the system, making the system analogous to a single-lined spectroscopic binary star. Accordingly, we used an automatic technique based on spectroscopic principal component analysis to search for broad H β emission lines that are displaced from the rest-frame of the quasar by $|\Delta v| \gtrsim 1,000 \text{ km s}^{-1}$ (corresponding to binary periods and separations of $P \sim \text{few} \times 100 \text{ yr}$ and $a \sim \text{few} \times 0.1 \text{ pc}$, respectively, for masses $\sim 10^8 M_{\odot}$). This method can also yield candidates for rapidly recoiling black holes since their spectroscopic signature is similar. Our search yielded 88 candidates, several of which were previously identified and discussed in the literature. The widths of the broad H β lines are typical among quasars but the shifts are extreme. We found a correlation between the peak offset and skewness of the broad H β profiles (there is an extended wing on the opposite side of the profile from the shifted peak), which suggests that the profiles we have selected share a common physical explanation. The general properties of the narrow emission lines are typical of quasars. We carried out followup spectroscopic observations of 68 objects to search for changes in the peak velocities of the H β lines (the time interval in the observer's frame between the original and new observations is 1–10 yr and 5.7–10.0 yr in 2/3 of the cases). We measured statistically significant changes (at 99% confidence) in 14 objects, with resulting accelerations between -120 and $+120 \text{ km s}^{-1} \text{ yr}^{-1}$. The above results, taken at face value, are broadly consistent with predictions for the number of close supermassive binaries in the Sloan Digital Sky Survey quasar sample. However, such a comparison is complicated by several theoretical and observational uncertainties, such as the fact that the observable we employ to select objects depends on a combination of several degenerate intrinsic parameters of a binary. We emphasize that interpretation of the offset broad emission lines as signatures of supermassive binaries is subject to many significant caveats. Many more followup observations over a long temporal baseline are needed to characterize the variability pattern of the broad lines and test that this pattern is indeed consistent with orbital motion. The possibility that some of the objects in this sample are rapidly recoiling black holes remains open as the available data do not provide strong constraints for this scenario.

All tables and two large figures in this preprint have been abridged. A version with all the figures and a complete list of the sample objects can be found at:

<http://www2.astro.psu.edu/users/mce/preprints/SBHB.pdf> (5 MB)

Subject headings: galaxies: active — (galaxies:) quasars: emission lines — (galaxies:) quasars: general — line: profiles

1. INTRODUCTION

1.1. *Theoretical Background and Motivation*

¹ Department of Astronomy and Astrophysics and Center for Gravitational Wave Physics, The Pennsylvania State University, 525 Davey Lab, University Park, PA 16803, U.S.A.

² Visiting Astronomer, Kitt Peak National Observatory, National Optical Astronomy Observatory, which is operated by the Association of Universities for Research in Astronomy (AURA) under cooperative agreement with the National Science Foundation.

³ National Optical Astronomy Observatory, Tucson, AZ 85719, U.S.A.

⁴ Columbia Astrophysics Laboratory, Columbia University, 550 West 120th Street, New York, NY 10027-6601, U.S.A.

The realization that the masses of the nuclear supermassive black holes (BHs) hosted by massive galaxies are related to the mass of the stellar spheroid of the host (e.g., Ferrarese & Merritt 2000; Gebhardt et al. 2000) has led to the development of new numerical and semi-analytic galaxy evolution models. Such models (e.g., Volonteri et al. 2003; Di Matteo et al. 2005; Hopkins et al. 2006) attribute the observed correlation to co-evolution of the black hole and the host via hierarchical galaxy mergers and accretion. Close supermassive black hole binaries (SBHBs) appear to be an inevitable stage in the evolution of the post-merger remnant. SBHBs have also been invoked to explain a variety of observations. Exam-

ples include stellar dynamical models that seek to explain the formation of cores in elliptical galaxies following a merger and mass deficits therein (e.g., Milosavljević et al. 2002; Merritt 2006), and the morphologies of some radio sources (such as precessing jets and X-shaped sources; see Roos, Kaastra, & Hummel 1993; Romero et al. 2000; Merritt & Ekers 2002; Gopal-Krishna, Biermann, & Wiita 2003). SBHBs are also expected to be among the primary sources of gravitational waves detectable by the Laser Interferometer Space Antenna (LISA; e.g., Sesana et al. 2005).

The evolution of SBHBs following the merger of their parent galaxies was first described by Begelman, Blandford, & Rees (1980). The early evolution (sinking of the BHs towards the center of the remnant and decay of the orbit via dynamical friction) proceeds relatively quickly, on a time scale comparable to the dynamical time of the parent galaxies ($\sim 10^8$ years). Once the binary “hardens” (i.e., the orbital speed becomes comparable to the stellar velocity dispersion) the evolution slows down as the orbital decay relies primarily on scattering of stars. If the number of stars whose orbits allow close encounters with the binary can be replenished efficiently, the process can shrink the orbit to a separation where the emission of gravitational waves becomes an effective orbital decay mechanism and the binary can coalesce within a Hubble time. However, it is still unknown whether this replenishment is possible via stellar dynamical processes (see, for example, discussions in Milosavljević & Merritt 2003; Berczik et al. 2006; Sesana, Haardt, & Madau 2007). Therefore, the possibility that the orbital evolution of the binary may stall at a separation $\lesssim 1$ pc remains open (this is known as “the last parsec problem”). Alternative mechanisms for the decay of the binary orbit have been explored in an effort to solve this problem, most notably drag by a large gaseous reservoir (e.g. a disk) or torques on a binary at short separations by a circumbinary disk (e.g. Escala et al. 2004; Dotti et al. 2007, 2009b; Cuadra et al. 2009; Lodato et al. 2009).

Despite their importance and the theoretical attention they have received, robust, *dynamical* evidence for the existence of large numbers of SBHBs at separations < 1 pc (the slowest phase in their evolution according to Begelman et al. 1980) remains elusive. Discovering such systems and obtaining a census of their population properties would serve as a test of galaxy evolution models and would provide valuable constraints for stellar and gas dynamical models for the decay of the binary orbit. It would also validate explanations of observed phenomena that appeal to such SBHBs.

The above evolutionary scenarios along with the new observational work on this subject (described below) have prompted the development of models for the observational signature of such binaries, such as the behavior of the emission lines from gas accreting onto the two BHs. The observational signature that is thought to provide the most direct, dynamical evidence for SBHBs is based on an analogy with spectroscopic binary stars. In this picture the emission lines from gas bound to one or both of the BHs (the broad-line region or BLR) are Doppler-shifted according to the line-of-sight velocity of the source. Bogdanović et al. (2008) have studied the interaction of the less massive (hereafter secondary) BH

with the accretion disk around the more massive (primary) one in a close, eccentric binary and have highlighted the potentially complex variability of the emission line profiles. Hayasaki, Mineshige, & Sudu (2007) and Cuadra et al. (2009) developed smoothed-particle hydrodynamic (SPH) models for the gas flow from a circumbinary disk onto disks around the individual BHs, based on which they make predictions about the relative accretion rates. In the context of such a picture of a binary within a circumbinary disk, Montuori et al. (2010) have used photoionization models to compute the relative strengths of the broad emission lines from these systems in an effort to devise spectroscopic diagnostics for SBHBs. Shen & Loeb (2010a) present a toy model of the BLRs in SBHB in which they employ test particles to represent clouds of gas in gravitationally bound orbits in the system and discuss its consequences for observational searches for SBHBs. Although this model is unrealistic⁵ and the predicted line profiles cannot be used as a basis for quantitative tests, the authors make the very important point that, at short separations the BLR would envelope the entire binary. This point was also made by M. Penston in 1988, as noted in footnote 3 of Chen, Halpern, & Filippenko (1989).

A related development in numerical relativity is the calculation of the recoil speed (or “kick”) of a BH resulting from the inspiral and merger of two BHs. A review of the recent literature on this subject can be found in Centrella et al. (2010a,b). The most extreme recoil speed expected from this effect is ~ 4000 km s⁻¹ for a special orientation of the spins of the two BHs relative to their orbital plane. However, under most other configurations, the recoil speed is considerably lower than this value (e.g., Campanelli et al. 2007a,b; Baker et al. 2008). As noted by Bogdanović, Reynolds, & Miller (2007), in a realistic astrophysical case the spins of the two BHs may be aligned with the orbital axis as a result of the previous evolution of the binary in a gaseous environment. In such a case, the recoil speeds would be rather low, namely of order a few hundred km s⁻¹. Indeed, Dotti et al. (2010) predict, based on detailed and extensive simulations, that the recoil speeds are likely to be distributed in the range 10–100 km s⁻¹.

As in the SBHB case, finding recoiling BHs and studying their population properties would be quite valuable. It would provide a test of calculations for the recoil speed but also much-needed constraints on models of the astrophysical implications for such kicks. A particularly interesting consequence of kicks is that they can propel the BH out of the host galaxy if they are strong enough (i.e., $\gtrsim 1,000$ km s⁻¹), which could influence the cosmological evolution of BHs (e.g., Volonteri et al. 2010). Otherwise, kicks can disturb the morphology of the host galaxy or offset an active nucleus from the center of its host (e.g., Gualandris & Merritt 2008; Komossa & Merritt 2008; Blecha et al. 2007). A potential observational signature of recoiling BHs is a Doppler

⁵ In addition to the shortcomings mentioned by the authors themselves, we also note that the basic premise of a BLR consisting of discrete clouds is not supported by observations (see, for example, Laor et al. 2006, and references therein). Even if a spherical system with crossing orbits like the one assumed could be set up, it would be destroyed by collisions on a very short time scale (see Mathews & Capriotti 1985).

shift of the broad emission lines originating in a BLR that is bound to the recoiling BH (see Loeb 2007). Another possibility is that the recoiling BH may accrete gas that it encounters along its trajectory, which could lead to a prolonged AGN phase lasting up to 0.1–1 Gyr Blecha et al. (2007). For large kicks, the spectroscopic signature of such a system is similar to the signature one might expect from some sub-parsec SBHBs, implying that a systematic search for SBHBs based on this idea may also yield useful constraints on the frequency of large kicks.

1.2. *Observational Searches for Close Binary and Recoiling Holes in Historical Perspective*

Until recently, direct imaging had resolved very few (presumably unbound) wide BH pairs, such as NGC 6240 (Komossa et al. 2003), and a close pair, CSO 0402+379 (Maness et al. 2004; Rodriguez et al. 2006, 2009). Recent spectroscopic surveys, however, have uncovered a substantial population of moderate-redshift AGNs with offset or double-peaked, narrow [O III] emission lines. Although some of the offset or double-peaked [O III] lines could arise in biconical outflows from single active nuclei (see Crenshaw et al. 2010), some of them turn out to trace dual active nuclei in merging galaxies, as shown by followup studies (e.g., Comerford et al. 2009a,b; Liu et al. 2010a,b; Shen et al. 2010b; Smith et al. 2010b; Fu et al. 2010). These dual active nuclei have separations of order a few kiloparsec (a representative example is COSMOS J100043.15+020637.2, reported by Comerford et al. 2009b).

In contrast, close, bound binaries, at sub-parsec separations, have been quite elusive as they cannot be resolved spatially. Nevertheless, such close binaries are of particular interest because they represent the slowest phase in the evolution of such a system, according to Begelman et al. (1980). In a well-known case, the ~ 12 -year periodic modulation in the long-term light curve of OJ 287 has been explained in terms of a close SBHB (e.g., Valtonen et al. 2008, and references therein). Other cases rely on a different type of indirect evidence, the detection of broad emission-lines with displaced peaks in quasar spectra. The underlying hypothesis here is that one or both of the two BHs in a SBHB has a gaseous BLR associated with it that emits the broad, permitted lines that are characteristic of quasar spectra. Thus, the orbital motion of the binary causes the lines to shift periodically making the spectrum analogous to that of a single- or double-lined spectroscopic binary star (see Komberg 1968; Begelman et al. 1980). In the context of this hypothesis, Gaskell (1983, 1984) identified two quasars, 3C 227 and Mrk 668, whose broad $H\beta$ emission lines were shifted from their nominal positions by 2,000–3,000 km s^{-1} and proposed that these are examples of close SBHBs in which only one of the two BLRs is visible. He also suggested that quasars with double-peaked emission lines, such as 3C 390.3, could represent SBHB in which both BLRs are visible. Indeed, an observed systematic drift of the blue-shifted, broad $H\beta$ peak in the spectrum of 3C 390.3 between 1968 and 1988 was consistent with this hypothesis (Gaskell 1996). However, this behavior is a rather uncommon feature of double-peaked emission lines (e.g., Gezari et al. 2007; Lewis et al. 2010) and, in fact, the trend observed in

3C 390.3 did not continue past 1990 (Eracleous et al. 1997; Shapovalova et al. 2001). Moreover, in a detailed study of the long-term variability of double-peaked emission lines in three quasars, Eracleous et al. (1997) did not detect the behavior expected from a binary BLR associated with an SBHB and also noted a number of contradictions between this interpretation and the observed properties of these objects. Finally, long-term variability studies of about two dozen double-peaked emitters (Gezari et al. 2007; Lewis et al. 2010) do not show the signature of orbital motion and a number of arguments suggest that broad double-peaked lines are much more likely to originate in an accretion disk (see discussion in Eracleous & Halpern 2003). Nevertheless, the binary black hole hypothesis remains a reasonable explanation for broad, *single-peaked* Balmer lines that are shifted from their nominal wavelengths. It is interesting that a number of such cases have been known for quite some time among nearby Seyfert galaxies. An inspection of the spectroscopic atlas of Stirpe (1990) reveals several examples, of which Mrk 876 and NGC 5548⁶ are particularly striking.

The recent theoretical work on the evolution of black holes in merging galaxies has been accompanied by new observational work directed at identifying close (sub-parsec) SBHBs. A handful of quasars from the Sloan Digital Sky Survey (SDSS), whose broad $H\beta$ lines have peaks that are displaced from their nominal wavelengths by a few thousand km s^{-1} , have been noted and discussed. The quasar SDSS J092712.65+294344.0 was interpreted as a SBHB by Bogdanović, Eracleous, & Sigurdsson (2009) and Dotti et al. (2009a), although it was proposed by Komossa, Zhou, & Liu (2008) as a candidate recoiling BH (see also our discussion below). The quasar SDSS J153636.22+044127.0 was identified by Boroson & Lauer (2009) who attributed its strong, broad, blueshifted $H\beta$ peak to a BLR around one of the members of a SBHB. However, Chornock et al. (2010) and Gaskell (2010) called this interpretation into question based on the presence of a prominent red shoulder in the $H\alpha$ profile, which is also discernible in the $H\beta$ profile, and suggested that the Balmer lines originate in a perturbed disk around a single black hole. Yet another interpretation for this object was offered by Tang & Grindlay (2009), who proposed that this quasar does harbor a SBHB and the profiles of the Balmer lines comprise contributions from an accretion disk around the primary BH, a BLR associated with the secondary BH, and a more extended gaseous region surrounding the binary. An interpretation similar to that of Tang & Grindlay (2009) was also discussed by Barrows et al. (2011) for the $H\beta$ profile of SDSS J093201.60+031858.7. A fourth case, 4C+22.25 (a.k.a. SDSS J100021.80+223318.7) was recently reported and discussed by Decarli et al. (2010). The $H\beta$ profile of this object is reminiscent of SDSS J092712.65+294344.0 (a broad peak blueshifted by 8,700 km s^{-1}), but the large blueshift of the peak makes a rapidly-recoiling BH interpretation untenable. In a

⁶ The variations of the $H\beta$ profile of NGC 5548 were discussed by Peterson, Korista, & Cota (1987) in the context of a SBHB model. However, the wealth of data available today indicate that the variability properties of this object do not support such an interpretation (e.g., Wanders & Peterson 1996; Peterson et al. 2002; Sergeev et al. 2007).

very recent study, Tsalamantza et al. (2011) have used an automatic method to search systematically through the SDSS DR7 spectroscopic database (including 54,586 objects classified as quasars and 3,929 objects classified as galaxies at $0.1 < z < 1.5$) for objects with displaced emission line peaks. They have uncovered five new SBHB candidates, in addition to the ones noted above. All of the above objects should be regarded as preliminary candidates for SBHBs in the absence of additional evidence. This is because our lack of understanding of the structure and properties of the BLR does not preclude that such unusual line profiles can originate from the BLR around a single BH. The case would be strengthened if the displaced peaks are observed to drift in time, as one would expect for the lines of a spectroscopic binary star.

A systematic search for recoiling BHs was undertaken only recently, motivated by the new developments in numerical relativity. Bonning et al. (2007) studied the distribution of shifts of the broad $H\beta$ lines in the SDSS DR3 quasar sample and found that shifts greater than 800 km s^{-1} occur in only 0.2% of cases, with progressively more stringent limits for larger shifts. The latest studies for the distribution of kicks (e.g., Dotti et al. 2010) suggest that the vast majority of recoil speeds should be $\lesssim 100 \text{ km s}^{-1}$, which means that recoiling BHs would not be easily identifiable in the sample of Bonning et al. (2007).

Three candidate *rapidly* recoiling black holes have been noted and discussed in the recent literature, but their cases are ambiguous or controversial. As we mentioned above, SDSS J092712.65+294344.0 was identified by Komossa et al. (2008) via its shifted $H\beta$ line, who suggested that this is a rapidly-recoiling black hole. However, a number of different interpretations were offered by followup papers, including a binary black hole (Bogdanović et al. 2009; Dotti et al. 2009a), a chance superposition of objects at different redshifts on the sky (Shields et al. 2009b), and a superposition of objects in the same, massive galaxy cluster (Heckman et al. 2009). Similarly SDSS J105041.35+345631.3 was discovered through a visual inspection of a large number of SDSS quasars and discussed by Shields et al. (2009a) and Smith et al. (2010a). These authors noted that the relatively symmetric displaced peaks of the Balmer lines suggest a rapidly recoiling BH but differences between the profiles of broad lines from different ions ($H\text{ I}$ and Mg II) suggests that the lines are actually double-peaked but extremely asymmetric, which would point to an origin in a perturbed accretion disk. Finally, Civano et al. (2010) suggested that one of the two nuclei CID-42 (a.k.a. COSMOS J100043.15+020637.2; see the first paragraph of this section) could also be a rapidly recoiling BH.

The ambiguity surrounding the objects mentioned in the previous paragraph stems from the fact that the available data do not allow us to definitively distinguish between SBHBs and rapidly recoiling BHs. The detection of a change in the velocity offset of the broad lines would favor the SBHB over the recoiling BH interpretation, although it would not provide iron-clad evidence, as we discuss in more detail in later sections of this paper. One can argue against a recoiling BH interpretation in some particular cases on theoretical grounds, since recoil speeds far in excess of 100 km s^{-1} are extremely unlikely

(e.g., Dotti et al. 2010) and speeds above $4,000 \text{ km s}^{-1}$ are unattainable (e.g., Campanelli et al. 2007a,b). An indirect test has been described by Bonning et al. (2007) and re-iterated by Shields et al. (2009a) in which the displaced broad lines have fairly symmetric profiles and the prominent narrow lines have similar widths, regardless of ionization state. The underlying hypothesis here is that the broad lines are emitted from an otherwise ordinary BLR that is attached to the recoiling BH (see Loeb 2007) and that the narrow lines are emitted from the galaxy where the BH originated, which is now illuminated from the outside.

2. SCOPE AND GOALS OF OUR PROGRAM AND CONSIDERATIONS UNDERLYING THE SELECTION OF CANDIDATES AND SEARCH STRATEGY

Motivated by the above, we have embarked on a systematic search for quasars whose broad (single-peaked) $H\beta$ lines are offset from their nominal wavelengths by $|\Delta v| \gtrsim 1,000 \text{ km s}^{-1}$. We regard such objects as candidates for close (sub-parsec) SBHBs or rapidly recoiling BHs and have begun followup observations to search for changes in the shifts of their broad lines. Even though we adopt this as our working hypothesis, we emphasize that such line profiles need not be signposts of SBHBs. One can envision scenarios in which such line profiles can originate from the BLR associated with a single BH that does not have a companion. Thus, the mere detection of an offset in the broad Balmer lines yields only weak candidates for SBHBs or rapidly recoiling BHs. The detection of gradual drifts in the broad Balmer lines via followup observations strengthens the case for a SBHB, but a convincing demonstration that a specific object harbors a SBHB requires us to observe (ideally) a few orbital cycles. We return to these issues in §7, where we offer a more extensive discussion.

Based on the models of Volonteri et al. (2009) we would optimistically expect up to ~ 160 sub-parsec SBHBs in the sample that we have searched. However, there are significant theoretical uncertainties and models by these authors based on different assumptions yield a number that is lower by an order of magnitude. Since the SBHB phase is thought to be considerably longer than the accretion phase of a recoiling BH and since the expected distribution of recoil speeds is heavily weighted towards low speeds ($|v| \ll 1,000 \text{ km s}^{-1}$) we expect that only a very small fraction of the the quasars we select will be candidate recoiling BHs (see Bogdanović et al. 2007; Dotti et al. 2009a, 2010).

If the binaries evolve within a large-scale gaseous disk, as suggested by recent theoretical studies (e.g., Dotti et al. 2007, 2009b), we would expect that their orbits will have circularized by the time they reach sub-parsec orbital separations. At this evolutionary stage, binaries open a hole at the center of the circumbinary disk and the secondary BH orbits closer to the gas reservoir and has easier access to it. Therefore, the accretion rate onto the secondary is considerably higher than that onto the primary (see the recent work by Hayasaki et al. 2007 and Cuadra et al. 2009, building on previous calculations by Artymowicz & Lubow 1996 and Gould & Rix 2000), which leads us to attribute any shifted emission lines we detect to a BLR associated with the secondary. The resonant interaction of the binary with the

circumbinary disk could lead to an increase in the eccentricity. This is a somewhat uncertain process, which depends on the thermodynamic properties of the circumbinary disk and the amount of gas accreted by the BHs (see Artymowicz et al. 1991; Armitage & Natarajan 2005; Cuadra et al. 2009; Rödiger et al. 2011). We consider the accreting secondary scenario to be more likely on theoretical grounds, but our technique does not preclude us from finding systems in which the BLR is associated with the primary (e.g. Chang et al. 2010), or systems with a BLR that envelops the entire binary.

Since the main observable we employ is the velocity offset of the broad H β line, we consider here how the properties of detectable binaries might depend on this quantity. For the sake of simplicity we assume that the orbit is circular. Following Bogdanović et al. (2009), we write the magnitude of the observed velocity shift (i.e., projected along the line of sight) of the broad lines from the BLR of the secondary, u_2 , in terms of the true orbital speed, V_2 , as $u_2 = V_2 \sin i |\sin \phi|$, where i is the inclination of the orbit ($i = 0^\circ$ is face on), $\phi = 2\pi(t - t_0)/P$ is the orbital phase, and P is the period. We express the period and orbital separation of the binary in terms of the total mass, $M_8 = (M_1 + M_2)/10^8 M_\odot$, mass ratio, $q = M_2/M_1 < 1$, and the projected velocity of the secondary, $u_{2,3} = u_2/10^3 \text{ km s}^{-1}$ as:

$$P = 2652 M_8 \left[\frac{\sin i |\sin \phi|}{(1+q) u_{2,3}} \right]^3 \text{ yr} \quad (1)$$

and

$$a = 0.432 M_8 \left[\frac{\sin i |\sin \phi|}{(1+q) u_{2,3}} \right]^2 \text{ pc}. \quad (2)$$

If the emission lines trace the motion of the primary instead, the above equations can be adapted by replacing $u_{2,3}$ by $u_{1,3}/q$, where $u_{1,3} = u_1/10^3 \text{ km s}^{-1}$ (u_1 is the projected speed of the primary). For the sake of estimating typical binary periods and separations, we set $i = \phi = 45^\circ$, which yields

$$P = \frac{332 M_8}{(1+q)^3 u_{2,3}^2} \left(\frac{\sin i}{\sin 45^\circ} \frac{|\sin \phi|}{\sin 45^\circ} \right)^3 \text{ yr} \quad (3)$$

and

$$a = \frac{0.11 M_8}{(1+q)^2 u_{2,3}^2} \left(\frac{\sin i}{\sin 45^\circ} \frac{|\sin \phi|}{\sin 45^\circ} \right)^2 \text{ pc}. \quad (4)$$

In other words, if we measure the projected speed of the secondary BH to be of order 10^3 km s^{-1} in a binary with $q \ll 1$ and $M_8 \sim 1$, then it is reasonable to expect the binary to have a period of order a few centuries and a sub-parsec separation. We note here that the mass of the secondary cannot be arbitrarily small since it is constrained by the requirement that the accretion luminosity be high enough for this object to appear as a quasar. If the emission lines trace the motion of the primary instead, then the period and separation would be smaller by factors of q^3 and q^2 , respectively. These long orbital periods highlight a significant difficulty in securely identifying SBHBs: orbital periods are very long compared to a human lifetime, hence the observation of even a single orbital cycle requires considerable patience and persistence. In an optimistic scenario, where the binary has a

mass and a projected velocity offset such that $M_8 \approx 0.1$ and $u_{2,3} \approx 2$, the orbital period could be as short as a decade, however. We will return to this issue in §7 where we will consider the likelihood of observing a system with a specific set of properties.

As we noted above, the case for a displaced broad line signaling the presence of a binary becomes stronger if the shift of the line is observed to change with time. In the context of the binary picture outlined in the previous paragraph, the projected acceleration is given by

$$\begin{aligned} \left| \frac{du_2}{dt} \right| &= 2.4 \frac{u_{2,3}^4 (1+q)^3}{M_8 \sin^3 i} \left| \frac{\cos \phi}{\sin^4 \phi} \right| \text{ km s}^{-1} \text{ yr}^{-1} \\ &= 19 \frac{u_{2,3}^4 (1+q)^3}{M_8} \left(\frac{\sin 45^\circ}{\sin i} \right)^3 \\ &\quad \times \frac{|\cos \phi|}{\cos 45^\circ} \left(\frac{\sin 45^\circ}{\sin \phi} \right)^4 \text{ km s}^{-1} \text{ yr}^{-1} \end{aligned} \quad (5)$$

The time intervals (in the observer's frame) between the original SDSS observations and the new observations carried out in our program are in the range of 5–10 years. Thus, for sub-parsec binaries with orbital periods of order centuries, it is reasonable to expect the line shifts to have changed by $100\text{--}200 \text{ km s}^{-1}$. Our survey was, therefore, designed to detect changes of this order. If, however, the broad line shifts trace the motion of the primary, then, *for a given observed velocity* the accelerations are larger by a factor of q^{-3} compared to the expression in equation (5) and are easier to detect.

It is noteworthy that $|du_j/dt| \propto V_j |\cos \phi|$, while $u_j \propto V_j |\sin \phi|$ (where $j = 1, 2$ labels the BH), i.e., the speed and acceleration are $\frac{1}{4}$ cycle out of phase during their oscillation. This means that binaries near conjunction should display small velocity offsets but large accelerations, while binaries near quadrature should display large velocity offsets and small accelerations. As noted by Bogdanović et al. (2009), this represents an inherent difficulty in making a case for a SBHB because large accelerations should be accompanied by small line shifts and vice versa.

With these considerations in mind, in §3 we describe in detail how we selected our sample out of the SDSS spectroscopic database and we present the basic properties of the resulting objects, while in §4 we present a detailed study of the spectroscopic properties of these objects. In §5 we present our followup (“2nd-epoch”) observations and compare the followup spectra to the SDSS spectra. The techniques we used to search for velocity changes in the displaced broad peaks are described in §6 and in §7 we summarize and discuss our results.

3. TARGET SELECTION

The basis for our identification of candidates for the target list is a principal component analysis (PCA) technique described in detail by Boroson & Lauer (2010). We applied this technique to the SDSS spectra of 15,900 QSOs having redshift $z < 0.7$, from the catalog of Schneider et al. (2010). We note that this catalog includes only objects more luminous than $M_i = -22$. The input variables were the spectra themselves, shifted to

rest and trimmed to the wavelength range 4290–5400 Å, centered roughly on the H β region. Eigenspectra were generated from a subset of these (1,000 objects) with the highest signal-to-noise. Although the spectrum of almost every object could be modeled to within its noise by using a large number of eigenspectra, our goal was to identify the objects with the worst fits as candidates for our sample. Thus, we reconstructed each of the 15,900 spectra using only the five most significant eigenspectra. This effectively limits the reconstruction such that it can only reproduce the most common features and characteristics of the line profiles.

We adopted a threshold of $\chi^2/\nu > 3$ (where ν is the number of degrees of freedom, i.e., the number of spectral pixels) as a starting point for identifying spectra that were fitted poorly and were therefore candidate offset-peak objects. This gave us 910 objects. Note that this threshold value is arbitrary and is dependent on the signal-to-noise ratio (S/N) of the spectrum. A very high- S/N spectrum with a slightly unusual line profile will result in a poor fit. However, we thought that this approach would tend to err on the side of including many objects that we would later reject, and so it is inherently conservative.

We visually inspected the 910 spectra identified by the automatic selection algorithm and applied the following additional criteria. We excluded most objects in which the peak of the broad H β line was shifted by less than 1,000 km s $^{-1}$ from the peak of the narrow H β line (interpreted as the systemic redshift) since any offset broad-line peak is blended with the narrow H β line and difficult to discern. Identifying the peak of the broad line was subjective in some cases, particularly in noisy spectra. We excluded H β profiles with shelves and inflections, if they had a dominant broad peak at $v \approx 0$ (examples of quasars with such profiles that were excluded are SDSS J121716.08+080942.0, SDSS J143452.45+483942.8, SDSS J154348.62+401324.9, and SDSS J154929.43+023701.1; see Figure 5 of Zamfir et al. 2010). We also excluded clear double-peaked emitters, i.e., objects with two clearly separated broad peaks on either side of the narrow H β line. This is because variability studies have tested and rejected the hypothesis that such profiles are indicative of SBHBs (Eracleous et al. 1997; Gezari et al. 2007; Lewis et al. 2010). However, we retained objects whose broad H β profiles have a strong displaced peak plus an extended wing or shoulder on the opposite side of the narrow H β line (a prime example of such an object is SDSS J153636.22+044127.0, presented by Boroson & Lauer 2009, while additional examples from our collection are identified in §4.3)⁷. We also retained flat-topped profiles, if these were not centered at $v = 0$ since they could be a manifestation of a single broad-line region bound to a SBHB (see Shen & Loeb 2010a). This

⁷ Objects with such profiles have been termed “extreme double-peaked emitters” and have been discussed as alternative interpretations for broad displaced peaks to SBHBs (e.g. Shields et al. 2009b; Lauer & Boroson 2009; Decarli et al. 2010). These two explanations are not mutually exclusive, of course. The unusual profiles of extreme double-peaked emitters could be the result of perturbation of the line-emitting disk from a companion BH in a SBHB (e.g., Eracleous et al. 1995; Bogdanović et al. 2008; Tang & Grindlay 2009). However, similar perturbations can be caused by the self gravity of the disk.

subjective, visual classification process resulted in a sample of 88 objects that met all our criteria. To these we added two more objects listed by Strateva et al. (2003), which had not been selected by our $\chi^2/\nu > 3$ condition. Again, we stress that this is not a complete sample in any sense, though we believe that it includes almost all of the objects that fit our criteria.

According to Volonteri et al. (2009) there may be up to 150 detectable SBHBs with $q > 0.01$ in the sample of 15,900 quasars we have searched. However, models based on different assumptions predict up to an order of magnitude lower numbers, and the predictions are, in fact, consistent with zero when theoretical uncertainties are considered.

The 88 objects making up the resulting sample, along with their basic properties are listed in Table 1. This sample is considerably larger than the few objects with case studies published so far. In columns 1–5 of this table we give the redshift, apparent V magnitude, Galactic V-band extinction in the direction of the source, and the absolute V magnitude for each quasar. These quantities were obtained as described in §4.1. Hereafter, we will adopt abbreviated designations for these objects using the first six digits of the right ascension (i.e., down to integer seconds, e.g., Jhhmmss). With this convention we can refer to the objects in Table 1 uniquely. In columns 6–10 of Table 1 we list the particulars of the spectroscopic observations of each target, starting with the original SDSS observations (additional rows refer to followup observations described in §5).

Some of the objects in Table 1 were identified previously and discussed by other authors, as follows.

- The quasar J140700 is Mrk 668, one of the first two candidate SBHBs proposed by Gaskell (1983). It is noteworthy that the other candidate SBHB of Gaskell (1983), 3C 227, was also observed during the SDSS (designated SDSS J094745.14+072520.5) but was not selected by our algorithm. This is because the profile of its broad H β line at the time of the SDSS spectroscopic observation (UT 2003/03/26) was relatively symmetric and centered at the nominal wavelength of the line. We will return to these two objects in our discussion of interesting cases in later sections of the paper.
- We have recovered three objects that have received attention in the recent literature: J092712 and J105041 (see §1.2), as well J153636 (originally discovered by this method). We have also recovered an object noted by Bonning et al. (2007), J091833⁸. In §4.2 we compare in more detail the properties of the broad H β lines from our sample to the findings of Bonning et al. (2007) and to statistical studies by other authors.
- Our sample has 13 objects in common with the list of 32 objects of Tsalamantza et al. (2011), who also used an automatic selection algorithm to search through the SDSS DR7 spectroscopic database. Of these 13 objects, four are the objects listed in the previous paragraph, two are newly selected SBHB

⁸ Bonning et al. (2007) drew attention to this object because it had the largest velocity offset in their sample

TABLE 1
LOG OF SPECTROSCOPIC OBSERVATIONS

Object Name SDSS J (1)	z^a (2)	m_V^b (mag) (3)	A_V^c (mag) (4)	M_V^d (mag) (5)	Observation Date (UT) (6)	Instr. Code ^e (7)	Exposure Time (s) (8)	S/N^f (9)	Rest-Frame Wavelength Range (Å) (10)
001224.02 – 102226.2	0.2287	17.07	0.127	–23.27	2001/08/20 2009/12/16	S M	3756 3600	29 28	3093–7505 3181–6165
002444.10 + 003221.3	0.4024	16.85	0.083	–24.86	2000/12/22 2009/12/18	S M	9900 2400	88 30	2709–6594 2811–5426
015530.01 – 085704.0	0.1648	16.84	0.080	–22.65	2001/09/16 2009/12/17	S M	2702 3600	32 55	3263–7917 3375–6524
020011.53 – 093126.2	0.3602	17.96	0.081	–23.46	2001/08/28 2009/12/17	S M	8104 3600	34 28	2795–6780 2890–5586
021259.59 – 003029.5	0.3945	17.87	0.117	–23.83	2000/09/29 2009/12/16	S M	2700 3600	29 13	2714–6613 2803–5433
022014.57 – 072859.1	0.2137	18.65	0.078	–21.47	2001/09/10 2009/12/16	S M	4501 3600	11 16	3133–7598 3220–6241

The remaining objects have been omitted
The full table can be found in the complete preprint

^a The redshift of the object as measured in this paper from the peak wavelength of [O III] λ 5007 line.

^b The apparent V magnitude, determined from the SDSS PSF magnitudes, as described in §4 of the text.

^c The Galactic visual extinction, taken from Schlegel, Finkbeiner, & Davis (1998)

^d The absolute V magnitude, computed as described in §4 of the text.

^e The telescope and instrument configuration, as described in Table 2.

^f The signal-to-noise ratio (S/N) in the continuum near the line of interest. When the spectrum includes the $H\beta$ line we give the S/N in the continuum near this line, at 4600 Å. If the spectrum includes only the Mg II λ 2800 line, we give the S/N in the continuum near this line, at 2900 Å.

TABLE 2
LIST OF TELESCOPES AND INSTRUMENTS

Instrument Code	Observatory, Telescope, and Spectrograph	Spectral Elements	Resolution ^a (Å)
S	SDSS 2.5m, SDSS spectrograph	640, 440 mm ⁻¹ grisms, $d = 3''$ fibers	2.7
M	MDM, Hiltner 2.4m, Boller & Chivens CCD spectrograph	G350L grating (150 mm ⁻¹), 1''0 slit	7.6
K	KPNO, Mayall 4m, Ritchie-Cretien spectrograph	KPC-007 grating (600 mm ⁻¹), 1''5 slit	3.1
Pb Pr	Palomar, Hale 5m, Double Spectrograph	blue arm: 600 mm ⁻¹ grating, 1''5 slit red arm: 600 mm ⁻¹ grating, 1''5 slit	4.0 3.1
H1 H2	Hobby-Eberly Telescope, Low-Resolution Spectrograph	G1 grism (300 mm ⁻¹), 1''5 slit G2 grism (600 mm ⁻¹), 1''5 slit	14.5 5.6

candidates by both us and them (J115449 and J171448), while the remaining seven are objects that we regard as SBHB candidates while they have classified as having asymmetric line profiles or “other.” There are four SBHB candidates in the list of Tsalamantza et al. (2011) that are not in our sample: J0932+0318, J1000+2233, J1012+2613, and J1539+3333 (using their naming convention). The second and third of these four they also classified as double-peaked emitters (we agree with this classification) which is why they are not included in our sample.

- Five of the objects in our sample, J001224,

J015530, J094603, J114755, and J120924 were noted by Zamfir et al. (2010) as unusual cases that illustrate the wide diversity of Balmer line profiles in quasars. Several other objects in the Zamfir et al. (2010) study are worthy of mention, because they are not included in our sample. Two objects, J101912 and J162345, are below the luminosity threshold of the Schneider et al. (2010) QSO list. Three objects, J074948, J084203, and J143511, have broad $H\beta$ lines with peaks that are less than 1,000 km s⁻¹ from the narrow $H\beta$ line. One of these appeared in our candidate list with a χ^2/ν value of 3.92 and was rejected upon visual

inspection. The other two had χ^2/ν values just below our cutoff.

- Nine of the objects in our sample are also in the sample of $z < 0.33$ quasars with double-peaked H α lines by Strateva et al. (2003), selected from the SDSS DR3. These are J001224, J022014, J074157, J081329, J093844, J110742, J115644, J143455, and J172711. Of these, J081329 and J172711 have Balmer-line profiles whose centroid is somewhat blueshifted and with a strong blue peak and a weak red shoulder. As such their classification is somewhat ambiguous. The remaining seven objects have very skewed Balmer-line profiles with one clearly displaced peak, but a second peak is not clearly present, making their classification as double-peaked emitters questionable. Thus, we have retained all of these objects in our sample. We note that J001224 was used as an illustrative example of SBHB candidate by Shen & Loeb (2010a).

In the next section we present the basic properties of the sample objects and we study their spectra, paying particular attention to the profiles of their H β lines.

4. PROPERTIES OF THE SAMPLE

4.1. SDSS Observations and Basic Properties of Sample Objects

The apparent V magnitudes of the sample quasars were determined from the SDSS PSF magnitudes in the g and r bands, using the transformation equations of Jester et al. (2005). We obtained the redshifts of the sample quasars by measuring the peak wavelength of the [O III] $\lambda 5007$ line and by adopting a rest vacuum wavelength of 5008.239 Å for this line (since the SDSS spectra are on a vacuum wavelength scale). From this redshift, we determined the distance modulus using the prescriptions of Hogg (1999)⁹, adopting the following cosmological parameters: $H_0 = 73 \text{ km s}^{-1} \text{ Mpc}^{-1}$, $\Omega_M = 0.27$, and $\Omega_\Lambda = 0.73$. Thus, we obtained the absolute V magnitudes, taking into account Galactic extinction (from Schlegel, Finkbeiner, & Davis 1998), but not K corrections. The redshift, apparent V magnitude, and absolute V magnitude distributions are shown in the histograms of Figure 1. We note that the median redshift of our targets is 0.32, while the full range of redshifts extends from 0.077 to 0.713.

In columns 6–10 of Table 1 we give a log of the spectroscopic observations of the objects in our sample, including the UT date of the observation, the telescope and instrument configuration, the exposure time, the signal-to-noise ratio in the spectrum (S/N), and the rest-frame wavelength range covered by the spectrum. The table includes a separate block for each object, with the first row of each block giving the particulars of the SDSS observations. The instrument configurations are summarized in Table 2. It is noteworthy that the spectral

resolution of the SDSS spectra varies with wavelength such that the velocity resolution improves linearly with the log of the wavelength (see the discussion and illustration in Appendix B and Figure 16 of Bernardi et al. 2003). Thus, in Table 2 we list the spectral resolution at 6400 Å, which corresponds to the location of the H β line for the median redshift of our sample. The S/N was determined from the fluctuations about the mean continuum level in a 50 Å wide window near the emission line of interest. In particular, when the spectrum includes the H β line we give the S/N in the continuum near this line, at 4600 Å ($\Delta v \approx -16,600 \text{ km s}^{-1}$ relative to H β). If the spectrum includes only the Mg II $\lambda 2800$ line, we give the S/N in the continuum near this line, at 2900 Å ($\Delta v \approx +10,500 \text{ km s}^{-1}$ relative to Mg II).

The spectra of the Mg II, H β , and H α lines of the objects in our sample are shown in Figure 2 on a common velocity scale. The broad-line spectra shown in this figure illustrate that it is easier to find broad displaced peaks in the H β profiles, especially when the displacement is small, because the peak of the broad H α profile is “contaminated” by the narrow H α + [N II] complex. For example, in J130534 and J140007, one can easily discern an offset broad peak in the H β but not in the H α profiles. Vice versa, the H α profiles show more clearly the shape of the red side of the profile where the H β line may suffer from severe contamination by the [O III] doublet. For example, in J075403, J091928, and J121113, what appears to be an extended red wing in the H β profile actually has the form of a shoulder or weak red peak in the H α profile. The profiles of the Mg II lines are very similar to the profiles of the Balmer lines. Specifically, there is no discernible misalignment of the peaks of the different lines with only one exception: J105203. One must keep in mind, however, that the contamination of the peak of the broad line by the narrow doublet is more severe than in the case of H β and comparable in severity to the case of H α . Moreover, since the Mg II lines are resonance lines, the profiles of the broad emission lines are often contaminated by associated *absorption* lines, which can be fairly strong.

4.2. Processing of SDSS Spectra and Emission-Line Measurements

To quantify the spectroscopic properties of our targets, we measured the properties of some of the strong narrow emission lines as well as the properties of the profiles of the broad H β lines from the SDSS spectra.

Specifically, we measured the integrated fluxes and full widths at half maximum (FWHM) of the following narrow lines: [Ne V] $\lambda 3426$, [O II] $\lambda 3726, 3729$, [Ne III] $\lambda 3869$, H β and [O III] $\lambda 5007$. The widths and relative strengths of the narrow lines, especially the high-ionization ones, can serve as tests of the rapidly recoiling BH hypothesis, as discussed, for example, by Bonning et al. (2007), Komossa et al. (2008) and Shields et al. (2009a). To isolate the lines, we fitted a low order polynomial to the local *effective* continuum. In the case of the H β and [O III] $\lambda 5007$, we used a continuum model that also includes the contribution of the Fe II lines, as we describe later in this section. The line fluxes were then determined by integrating the observed line profile, while the widths were determined by fitting a Gaussian to the line

⁹ We used a program written by Benjamin Weiner, which is publically available at <http://mingus.as.arizona.edu/~bjw/software/>. We compared the luminosity distances from this program to those of Ned Wright’s cosmology calculator, available at <http://www.astro.ucla.edu/~Tewright/CosmoCalc.html>, and found them to agree within 0.1%.

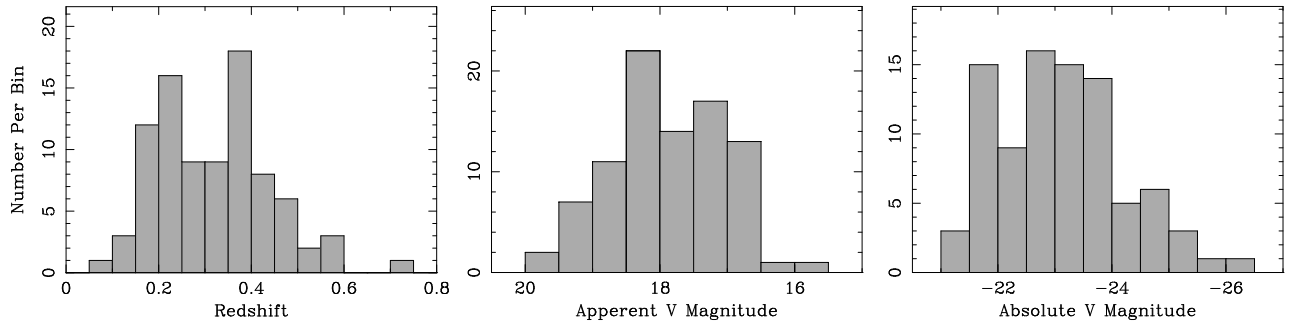


FIG. 1.— Distribution of the basic properties of the objects in our sample. The redshifts were determined from the wavelengths of the [O III] $\lambda 5007$ line. The apparent V magnitudes correspond to the PSF magnitude obtained from SDSS images. The absolute V magnitudes take into account Galactic extinction towards the source. Further details are given in §4.1 of the text.

profile and then correcting the FWHM for the finite resolution of the spectrograph at the observed wavelength of the line (see Appendix B and Figure 16 of Bernardi et al. 2003). We made no effort to de-blend the two lines in the [O II] $\lambda\lambda 3726, 3729$ doublet, therefore we do not report their widths. However, we did measure the width of the blended doublet, which allows us to discern in some cases whether the [O II] lines are narrower than other forbidden lines. The observed line fluxes were corrected for Galactic extinction using the values of A_V listed in Table 1 and assuming the extinction law of Seaton (1979). The resulting measurements are reported in Table 3 where we give the line fluxes relative to that of the [O III] $\lambda 5007$ line before and after extinction corrections, the observed and corrected [O III] $\lambda 5007$ flux, and the corrected [O III] $\lambda 5007$ luminosity, as well as the FWHM of the lines.

In order to isolate the profiles of the broad $H\beta$ lines we first subtracted a model of the underlying continuum and Fe II multiplets, which was fitted to the spectral range 4,000–5700 Å. The underlying continuum consisted of a linear combination of a starlight template and a featureless power law while the Fe II multiplets were modeled by suitably broadening a template, as described in Boroson & Green (1992). As a last step we subtracted the narrow $H\beta$ and [O III] lines by using the profile of the [O III] $\lambda 5007$ line as a template for the other two lines. As a cross-check, we used the profile of the [O III] $\lambda 4959$ as a template to subtract the [O III] $\lambda 5007$ line. The resulting broad $H\beta$ profiles are shown on a common velocity scale in Figure 3.

After isolating the broad $H\beta$ line profiles we quantified their shapes by measuring some of their central moments and related quantities. The n^{th} central moment of a line profile, μ_n , is defined in terms of the wavelengths and flux densities of the discrete pixels in the line profiles (λ_i and f_i respectively) as $\mu_n \equiv K \sum (\lambda_i - \langle \lambda \rangle)^n f_i$, where K is a normalization constant defined by $1/K = \sum f_i$ and $\langle \lambda \rangle \equiv K \sum \lambda_i f_i$ is the first moment or *centroid* of the line profile. Using the second and third central moments we determined the standard deviation and skewness of the line profiles as $\sigma = \mu_2^{1/2}$ and $s = \mu_3/\mu_2^{3/2}$, respectively. We also determined the Pearson skewness coefficient, defined as $p = (\langle \lambda \rangle - \lambda_m)/\sigma$, where λ_m is the median wavelength¹⁰. In Table 4 we report the centroid velocity shift relative to the nominal wavelength of $H\beta$ using the relativistic Doppler formula, the velocity

dispersion of the line, computed from the standard deviation as $c\sigma/\lambda_0$ (where λ_0 is the nominal wavelength of $H\beta$ and c is the speed of light), the skewness, and the Pearson skewness coefficient.

In addition to the above quantities, we also measured the velocity offset of the peak of the broad line and its FWHM, which we also report in Table 4. In order to make these measurements, we had to locate the peak of the broad line, which is somewhat subjective since the observed profiles have a finite S/N . Thus we attempted to determine the location of the peak of the broad line profile by fitting it with a Gaussian. This procedure leads to an uncertainty because the symmetric Gaussian does not always fit the line peak well, especially when the peak is asymmetric. To quantify this uncertainty, we made several measurements of the same line, varying the region around the peak used for the fit. In the end we adopted the maximum and minimum peak wavelengths from our trials to define the range of possible values and took their average as the best estimate of the peak wavelength. Thus, in Table 4 we report the velocity offset of the peak, computed from the relativistic Doppler formula, as well as its uncertainty. Finally, the FWHM was determined based on the height of the peak and expressed as a velocity width in the same manner.

4.3. Demographics and Statistical Properties of the Broad $H\beta$ Profiles and the Narrow Lines

Figure 4 illustrates the distribution of shifts of the peaks of the broad $H\beta$ lines among objects in our sample. The dearth of objects in the range ± 500 km s⁻¹ is a result of the fact that we purposely excluded most objects with such small shifts. In the same figure we show the range of shifts (± 3 standard deviations about a mean of 100 km s⁻¹) measured by Bonning et al. (2007), who studied the $H\beta$ profiles of 2598 quasars at $0.1 < z < 0.81$ drawn from a sample of approximately 13,000 objects from the SDSS DR5 and found 9 cases of large offsets, from $\approx 1,000$ km s⁻¹ to a maximum of 2,667 km s⁻¹. Our study appears to complement and supplement theirs since we recover a substantially larger number of highly offset peaks: 32 objects with $|\Delta v| > 1500$ km s⁻¹, a factor of 8 larger than what we would predict just by scaling the sample sizes. Similar conclusions follow if we compare our results with those of Zamfir et al. (2010), who studied the high- S/N spectra of 469 quasars with $z < 0.7$ from the SDSS DR5. The vast majority of our objects belong to their population B ($\text{FWHM}_{H\beta} > 4,000$ km s⁻¹, weak Fe II lines; see Sulentic et al. 2002), whose dis-

¹⁰ Because of the definitions we adopted for s and p , $s \propto -p$.

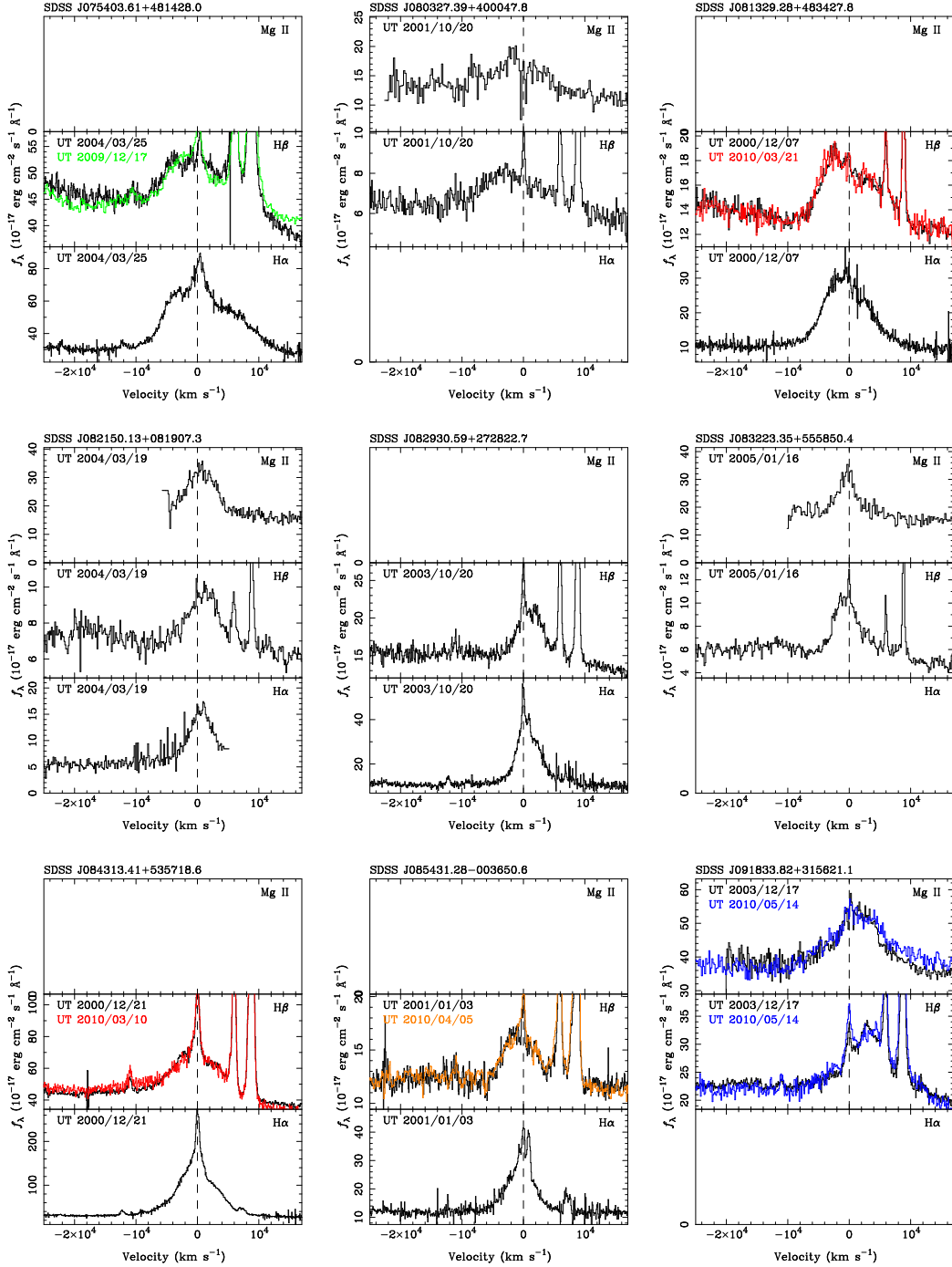


FIG. 2.— **ABRIDGED** Mg II, H β , and H α spectra of our target objects. For each object we show a 3-panel figure with the profiles of all three lines on a common velocity scale. The original SDSS spectra are plotted in black, while the post-SDSS spectra are color-coded as follows: KPNO 4m spectra are in red, Palomar 5m spectra are in blue, MDM 2.4m spectra are in green, and HET spectra are in orange. For the purpose of this illustration, some spectra were binned to increase the S/N per bin. The vertical scale was adjusted specifically for the original SDSS spectra. Post-SDSS spectra have been scaled and shifted so that the profiles of the broad lines match those of the SDSS spectra as closely as possible; see equation (6) and §5.2 of the text. As a result of this scaling, there is an apparent difference in the strengths of the narrow lines, if the flux of the broad line has varied between epochs.

TABLE 3
PROPERTIES OF NARROW EMISSION LINES

Object (1)	Obs. Flux Relative to [O III] ^a				Obs. $F_{[\text{O III}]}$ ^a	Corr. Flux Relative to [O III] ^b				Corr. $F_{[\text{O III}]}$ ^b	$L_{[\text{O III}]}$ ^c	FWHM (km s ⁻¹) ^d			
	[Ne V] (2)	[O II] (3)	[Ne III] (4)	H β (5)		[Ne V] (7)	[O II] (8)	[Ne III] (9)	H β (10)			[Ne V] (13)	[Ne III] (14)	H β (15)	[O III] (16)
J001224	<0.055	0.462	0.346	0.128	3.59	<0.058	0.483	0.359	0.129	3.95	5.73	...	910	510	540
J002444	0.200	0.130	0.242	0.193	7.77	0.207	0.133	0.247	0.194	8.19	44.0	890	910	420	420
J015530	0.157	0.166	0.184	0.237	16.9	0.162	0.171	0.189	0.238	18.0	12.5	670	550	470	290
J020011	<0.105	0.140	0.220	0.215	3.58	<0.109	0.143	0.225	0.215	3.77	15.5	...	1150	720	800
J021259	0.054	0.132	0.086	0.075	31.5	0.056	0.137	0.089	0.075	34.0	174.	430	490	450	440
J022014	<0.112	0.564	0.151	0.219	3.90	<0.116	0.579	0.155	0.220	4.14	5.14	...	560	400	370

The remaining objects have been omitted

^a Integrated line fluxes are expressed relative to the integrated flux of the [O III] λ 5007 line in units of 10^{-15} erg cm⁻² s⁻¹, as measured from the observed spectrum, without any corrections. The uncertainty is 5% or less, unless otherwise noted.

^b Integrated line fluxes are expressed relative to the integrated flux of the [O III] λ 5007 line in units of 10^{-15} erg cm⁻² s⁻¹, after correcting for Galactic extinction, as described in §4.2 of the text. The uncertainty is 5% or less, unless otherwise noted.

^c The luminosity of the [O III] λ 5007 line in units of 10^{37} erg s⁻¹, after correcting for Galactic extinction (see §4.2 of the text).

^d The full width at half maximum of the emission lines, corrected for the finite resolution of the spectrograph as described in §4.2 of the text. The value is omitted when the line is not detected.

^e The uncertainty in these measurements is 10–15%

^f The spectrum of J092712 includes two sets of narrow lines therefore we report the properties of each set in separate rows. The first row gives the properties of the set that is blueshifted and appears to be at the same redshift as the broad lines. The second row gives the properties of the set that is redshifted and has no broad lines associated with it.

TABLE 4
PROPERTIES OF BROAD H β PROFILES

Object (1)	FWHM (km s ⁻¹) (2)	FWQM (km s ⁻¹) (3)	Peak Velocity Shift (km s ⁻¹) (4)	Centroid Velocity Shift (km s ⁻¹) (5)	Velocity Dispersion (km s ⁻¹) (6)	Skewness Coefficient (7)	Pearson Skewness Coefficient (8)
J001224	3590	8630	-1870 \pm 80	280	3530	0.253	-0.197
J002444	9320	13450	-720 \pm 150	-80	3720	0.113	-0.056
J015530	7320	9180	1430 \pm 130	610	3100	-0.039	0.045
J020011	7660	12490	1650 \pm 60	460	3570	0.333	0.025
J021259	7990	11570	-2300 \pm 40	-10	3830	0.323	-0.106
J022014	8210	10560	-470 \pm 90	950	3240	0.495	-0.102

The remaining objects have been omitted

^a The redshift of the object as measured in this paper from the peak wavelength of [O III] λ 5007 line.

^b The apparent V magnitude, determined from the SDSS PSF magnitudes, as described in §4 of the text.

^c The Galactic visual extinction, taken from Schlegel, Finkbeiner, & Davis (1998)

^d The absolute V magnitude, computed as described in §4 of the text.

^e The telescope and instrument configuration, as described in Table 2.

^f The signal-to-noise ratio (S/N) in the continuum near the line of interest. When the spectrum includes the H β line we give the S/N in the continuum near this line, at 4600 Å. If the spectrum includes only the Mg II λ 2800 line, we give the S/N in the continuum near this line, at 2900 Å.

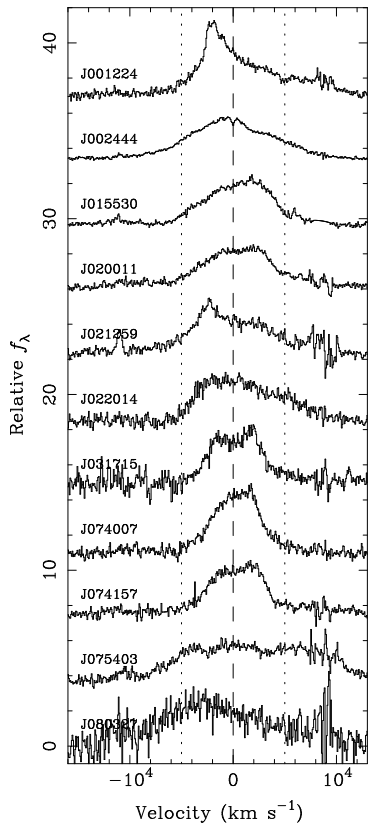


FIG. 3.— **ABRIDGED** Profiles of the broad $H\beta$ lines from the SDSS spectra, shown on a common velocity scale. The narrow $H\beta$ and $[O\text{ III}]$ lines and underlying continuum were subtracted as described in §4.2 of the text. The resulting profiles were normalized arbitrarily and offset vertically from each other for clarity. The vertical dashed line shows the location of the narrow $H\beta$ line, while the vertical dotted lines identify a window of $\pm 5,000\text{ km s}^{-1}$ from this line. The noise often seen at $+8875\text{ km s}^{-1}$ is a result of imperfect subtraction of the $[O\text{ III}] \lambda 5007$ line. The $\text{He II } \lambda 4686$ line, which was not subtracted, is sometimes discernible at $-10,800\text{ km s}^{-1}$.

tribution of broad $H\beta$ shifts shows some preference for redshifts and has extrema of $\pm 3100\text{ km s}^{-1}$. Thus, the objects we have identified here occupy the wings of the distribution of shifts of the peak of the broad $H\beta$ line.

Perusal of Figures 2 and 3 leads us to classify the Balmer line profiles into three broad families according to their shapes. The first family includes profiles whose widths are smaller than average and visual inspection does not show them to be particularly asymmetric. Two of the objects discussed extensively in the recent literature, J092712 and J105041, are prime examples of objects in this family. Additional examples include J082930, J095036, J110050, J122811, J132704, and J162914. The second family includes skewed profiles showing an extended wing or a shoulder on the side opposite from the direction of their displacement (e.g., profiles with a blue-shifted peak with an extended red wing or a weak red shoulder). Representative examples of this family with blue-shifted peaks (and red asymmetries) are J001224, J091928, J115449, J123001, J125809, J133432, J152942, J153636, while examples with red-shifted peaks (and blue asymmetries) include J015530, J093653, J094603, J113651, J130534, J143455. The third family includes objects with flat-topped profiles, such as J020011, J031715, J074157, J095539, J112751, J154340,

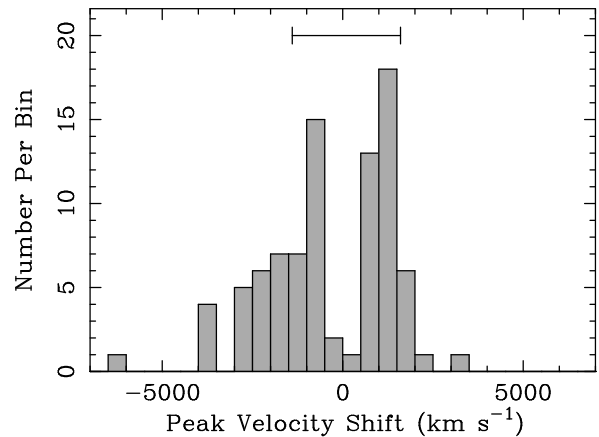


FIG. 4.— Distribution of the velocity shifts of the peaks of the broad $H\beta$, measured as described in §4.2 of the text. The dearth of objects in the range $\pm 500\text{ km s}^{-1}$ is a selection effect resulting from our inability to detect such small shifts with our method. The horizontal error bar at the top of the frame indicates the range of shifts found by Bonning et al. (2007): ± 3 standard deviations about a mean of 100 km s^{-1} .

J163020.

In addition to the visual classification of line profiles we have also looked for trends in their quantitative properties and we found a correlation between their shift and their skewness. We illustrate this correlation in Figure 5, where we plot the Pearson skewness coefficient *vs* the peak shift. A similar correlation is recovered when we consider other pairs of quantities that track skewness and shift, such as the skewness coefficient and the centroid shift. As the shift of the lines increases, the profile becomes more skewed. Moreover, the asymmetry manifests itself as an extended wing or weak shoulder on the side of the line profile that is *opposite* from the direction of the shift, with the result that the sign of the skewness tracks the sign of the shift. This correlation quantifies the trend we noted in the second family of line profiles in the previous paragraph. We have not found any correlation between the FWHM of the lines and the shift of their peaks nor between any other pairs of quantities that track width and shift. Bonning et al. (2007) do report that $H\beta$ profiles with large shifts also have large FWHM but the vast majority of objects in their sample show considerably smaller $H\beta$ shifts than the objects we regard as large and the shifts they regard as large are considerably smaller than the shifts we measure. Therefore, our results are not at odds with theirs. We did find a weak correlation between the width and the skewness. These correlations are consistent with the findings of Zamfir et al. (2010), shown in their Figures 6a and 6c.

In Figures 6 and 7 we present the distribution of relative intensities and FWHM of the the narrow lines using the measurements presented in Table 3. The relative intensity distributions resemble very closely those of Seyfert 1 and Seyfert 1.5 galaxies in the compilation of Nagao et al. (2001), which suggests that the ionization parameter and the shape of the ionizing continuum are similar to those of Seyfert galaxies. The distribution of FWHM of the narrow lines is similar to what is observed in Seyfert galaxies (see Whittle 1985; Moore, Cohen, & Marcy 1996) and is also evident in the composite quasar spectrum of Vanden Berk et al. (2001). The average FWHM of the $[O\text{ III}]$ line is very similar to

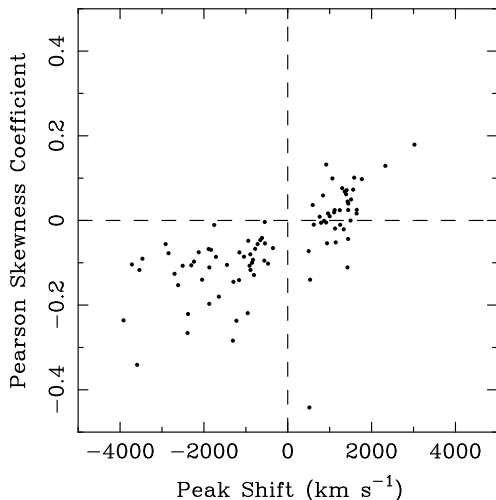


FIG. 5.— Relation between the skewness of the broad $H\beta$ profiles and the shift of their peaks. The Pearson skewness coefficient and the shift of the peak were measured as described in §4.2 and are tabulated in Table 4.

that found by Salvander et al. (2007) in their study of the spectra of 1736 quasars from SDSS DR3. Both the $[\text{Ne V}]$ and $[\text{Ne III}]$ lines in our sample are broader than $[\text{O III}]$, on average, and the $[\text{Ne V}]$ lines are always as broad as or broader than the $[\text{O III}]$ line within errors. This trend follows the correlation between FWHM and critical density noted for Syeferts (Filippenko & Halpern 1984; Whittle 1985). Thus the objects in our collection do not appear to stand out from typical active galactic nuclei as far as the properties of the narrow lines are concerned.

5. FOLLOWUP OBSERVATIONS AND NEW SPECTRA

5.1. Data Acquisition and Reduction

We carried out followup observations of 68 objects from our sample using four different telescopes: the brightest objects were observed with the 2.4m Hiltner telescope at MDM observatory, objects of intermediate brightness were observed with the 4m Mayall telescope at Kitt Peak National Observatory and the 5m Hale telescope at Palomar Observatory, while the faintest objects were observed with the 9.2m Hobby-Eberly Telescope (HET). With the followup observations we specifically targeted the $H\beta$ lines of the target objects, although we also did attempt to obtain spectra of the $H\alpha$ and Mg II lines whenever possible. The spectrographs and configurations we used for the observations are summarized in Table 2, along with the spectral resolution that each configuration can attain. The log of observations is included in Table 1 where, in addition to the observation date and exposure time, we also report the rest-frame wavelength range covered by each spectrum and the S/N achieved in the continuum near the line of interest (measured as described in §3, above). The weather conditions were varied during the followup observations and some spectra were taken through clouds. As a result, there are instances where we obtained a lower S/N than the original SDSS spectrum of the same objects in a comparable exposure time.

The spectra were reduced in a standard manner using

IRAF¹¹ for the first steps of the reduction process (bias subtraction, flat field division, sky subtraction, and extraction of raw spectra) and our own programs for the subsequent calibration (wavelength calibration, correction for continuous atmospheric extinction and discrete absorption bands, and flux calibration). Accurate wavelength calibration is important for our purposes since we aim to look for shifts in the $H\beta$ lines between the SDSS and post-SDSS spectra; thus we give here the details of the process. To obtain the transformation between pixel number and observed (air) wavelength we fitted a polynomial to the table of arc line pixel location *vs* wavelength. Depending on the instrument, we used 20–65 arc lines and achieved a fit with root-mean-square (r.m.s.) residuals of better than 0.10 pixels with a polynomial of order 4 or lower. Thus, the relative wavelength scale is good to 10 km s^{-1} for the KPNO 4m and Palomar 5m spectra, 13 km s^{-1} for the HET spectra and 18 km s^{-1} for the MDM 2.4m spectra. In comparison, the relative wavelength scale of the SDSS spectra is good to 0.07 pixels or 5 km s^{-1} (r.m.s.). After the spectra were fully calibrated, we applied heliocentric corrections (amounting to 0.15 \AA or less) and converted the wavelength scale from air wavelengths to vacuum wavelengths, following the convention for SDSS spectra. For the last step we used the relation between vacuum and air wavelengths given by Morton (1991), which yields corrections between approximately 0.5 and 2.5 \AA over the wavelength range of our spectra. With these corrections the r.m.s. shift between the SDSS and post-SDSS spectra amounted to 0.67 \AA or 41 km s^{-1} , determined by cross-correlation of the spectra over the region around the $[\text{O III}] \lambda\lambda 4959, 5007$ lines. Thus, in a final step we refined the alignment of spectra by rectifying these residual shifts. The final alignment is limited by our ability to determine the shift of the $[\text{O III}]$ lines by cross-correlation. In about 80% of the cases the r.m.s. alignment uncertainty is 7 km s^{-1} or better, while in the other 20% of cases it lies between 7 and 25 km s^{-1} .

5.2. Qualitative Comparison of New and Old Spectra

The distribution of time intervals (in the observer’s frame) between the original SDSS observations and the followup observations is shown in Figure 8. The median of the time interval distribution is 7.0 years, with 70% of the objects having a time interval between observations of at least 5.7 years.

In Figure 2 we overplot the post-SDSS spectra on the original SDSS spectra for comparison. Since our primary goal is to look for changes in the profiles of the broad emission lines, we have scaled and shifted the post-SDSS spectra so as to match these profiles as closely as possible. We applied a transformation to the flux density scale of the form

$$f'_{\lambda} = af_{\lambda} + b_{\lambda}, \quad (6)$$

where a and b_{λ} are constants, determined by minimizing the differences between the SDSS and post-SDSS spectra in selected regions of the broad line profiles and the

¹¹ IRAF, the Interactive Reduction and Analysis Facility, is distributed by the National Optical Astronomy Observatory, which is operated by the Association of Universities for Research in Astronomy (AURA) under cooperative agreement with the National Science Foundation (see <http://iraf.noao.edu/>).

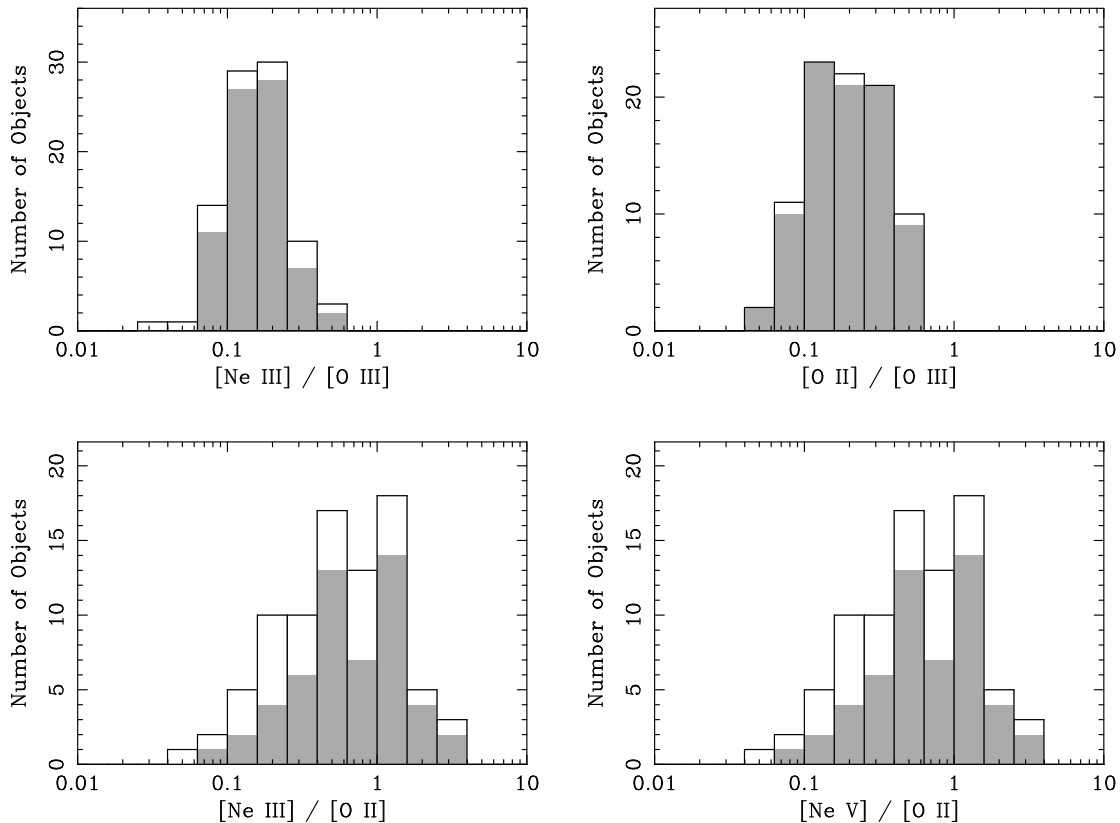


FIG. 6.— Distribution of four different narrow-line ratios among the quasars in our sample, after correction for Galactic extinction. The measurements were made from the SDSS spectra, as described in §4.2 of the text, and the results are tabulated in Table 3. The shaded portions of bins represent actual measurements while the hollow portions represent limits.

adjacent continuum. This scaling convention highlights changes in the profiles of the two spectra but it hides changes in the flux of the broad line and the continuum. Changes in the flux of the broad line can still be discerned by examining the intensities of the narrow lines (most notably [O III]), which are not expected to change in the time interval between observations. In other words an apparent mismatch in the strength of the narrow lines between two spectra indicates that flux of the broad line has changed between observations.

An inspection of Figure 2 reveals changes in the broad $H\beta$ lines between the SDSS and post-SDSS observations in many cases. Changes in the profile shapes are the easiest to discern. Examples of objects displaying this type of variability include J093653, J112751, J113706, J140700, and J143123. There are also several cases of changes in the integrated flux of the line, discernible through mismatches in the strengths of the [O III] lines, including but not limited to J021259, J094603, J111329, J115449, J132704, and J143455. Yet another category of changes comprises cases where the broad line has shifted in wavelength/velocity by a small amount. The most obvious example of such a change is J095036, while J094603, J140251, and J180545 represent examples of more subtle shifts of this type. This type of variability if, of course, of particular interest here, therefore we study it further in §6, below.

6. SEARCH FOR VELOCITY CHANGES IN THE BROAD $H\beta$ PROFILES

6.1. A χ^2 Cross-Correlation Method for Determining Velocity Changes

To determine any changes in the velocities the offset peaks of the broad $H\beta$ lines between the SDSS and post-SDSS spectra we developed an algorithm that is a variant of the standard cross-correlation method. In our method we shift one of the two spectra in small steps and at each step we compare it with the other spectrum via the χ^2 test. Based on several tests, we prefer this method over the standard cross-correlation (which employs the overlap integral rather than the χ^2 test at each step) for the following reasons: (a) it allows us to check whether the profile of the $H\beta$ line has changed between epochs (this is important because small changes in the profile can mimic a velocity change), (b) the χ^2 minimum is much sharper and deeper than the overlap integral maximum, thus easier to locate, especially if we are relying on the wings of the broad line for our comparison, (c) it allows us to determine uncertainties and limits on the shift in a more straightforward and less computationally intensive way, without the need for extensive simulations for each pair of spectra being compared.

Our χ^2 cross-correlation method is applied to a pair of spectra as follows: before any comparison is made, a linear transformation is applied to the flux scale of the second spectrum of the pair following equation (6), in order to match the continuum and the broad $H\beta$ line. This transformation creates a mismatch in the narrow lines, of course, but it allows us to carry out a direct comparison of the broad lines, without subtracting the continuum or the narrow lines, which would introduce additional sys-

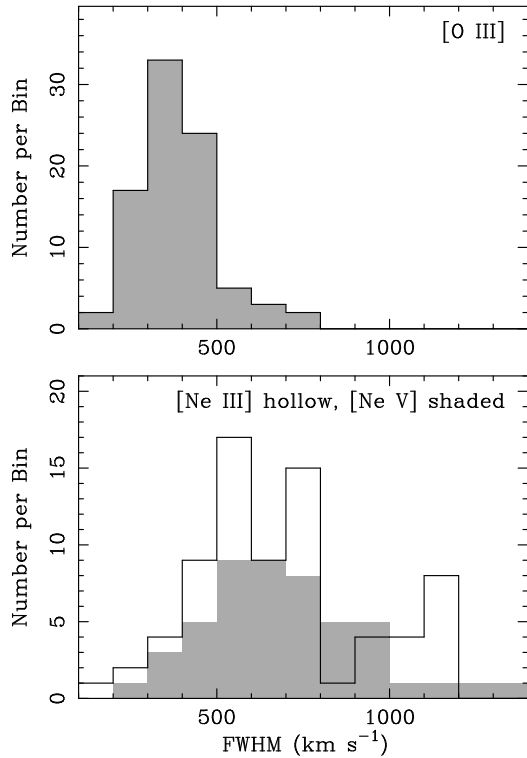


FIG. 7.— Distribution of the FWHM of high-excitation narrow lines of quasars in our sample, after correction for the finite resolution of the spectrograph. The measurements were made from the SDSS spectra, as described in §4.2 of the text, and the results are tabulated in Table 3. The upper panel shows the distribution of widths of the [O III] $\lambda 5007$ lines, while the lower panel shows the distributions of [Ne III] $\lambda 3869$ (black, solid line with hollow bins) and [Ne V] $\lambda 3426$ (shaded bins with no outline).

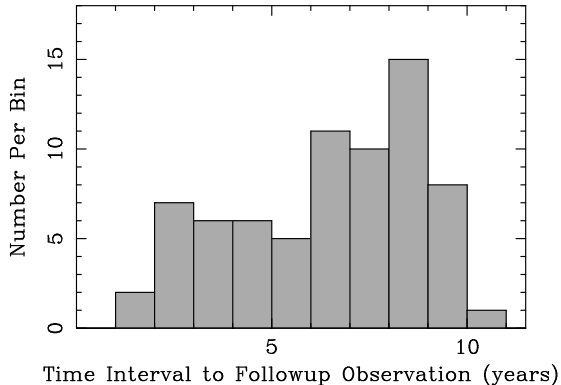


FIG. 8.— Distribution of the time intervals (in the observer’s frame) between the original SDSS spectra and the followup spectra obtained here. The median of this distribution is 7.0 years. For 70% of the objects the time interval between observations is at least 5.7 years.

tematic errors. The wavelength scale of the second spectrum is then shifted in small steps (typically $0.1\text{--}0.2 \text{ \AA}$), rebinned to the wavelength scale of the first spectrum, and finally the χ^2 statistic is evaluated to compare the profiles of the broad $H\beta$ lines in one or two windows that are not affected by narrow lines. These windows are chosen to encompass the offset broad peak and/or the steep wings or shoulders of the line so as to maximize the sensitivity to small shifts. The final output is a χ^2 curve as a function of shift. The minimum of this curve, determined

by fitting a parabola to the five lowest points, represents the optimal wavelength shift. The 99% (or “ 2.6σ ”) confidence interval about the minimum (for one interesting parameter) is determined by finding the shifts that correspond to $\chi^2_{\min} + 6.63$ (see Lampton, Margon, & Bowyer 1976). In Figure 9 we show graphically the application of this technique in three example cases, a shift that is statistically significant, a shift that is not statistically significant, and an apparent shift that is caused by a variation in the broad $H\beta$ profile between the two epochs.

We verified through simulations that $\chi^2_{\min} + 6.63$ does indeed reflect the 99% confidence interval. Each simulation was carried out by creating a copy of an observed high- S/N spectrum, adding synthetic noise, and then measuring the shift between the two spectra. We repeated this test for several examples of observed spectra from our collection. In 1000 realizations in each case we found that about 1% of the optimal shifts departed from zero by more than the amount predicted by the $\chi^2_{\min} + 6.63$ condition, as expected. An additional check of the procedure was carried out by switching the order of the spectra supplied to the χ^2 cross-correlation algorithm and comparing the resulting shifts. Indeed the distribution of discrepancies between the two shifts, normalized by the 99% confidence error bar was found to be approximately Gaussian with a standard deviation of $1/2.6$, as expected.

6.2. Application of the χ^2 Cross-Correlation Method and Results

We applied the above method to identify variable velocity candidates which we then scrutinized carefully to ensure that the shifts were genuine. We rejected cases where substantial variations of the broad line profiles mimic shifts (see example in Figure 9). We screened the initial candidates as follows: First we checked that the result was the same regardless of which of the two spectra was shifted and rebinned in the cross-correlation procedure (if more than one followup observation was carried out we also compared the results from the different observations). Then we inspected the spectra to ensure that the shift could be identified visually. In cases where the shift was subtle, we experimented by varying the spectral windows over which the χ^2 statistic was computed in order to verify that the result was robust. Finally, for the candidates that passed the above tests, we carried out simulations to verify the uncertainties: we made a copy of the spectrum with the higher- S/N added synthetic noise to match that of the lower- S/N spectrum and then applied the cross-correlation algorithm. After 1000 realizations we examined the distribution of shifts about zero to verify that the statistical uncertainty in the shift was not underestimated. After arriving at the final statistical uncertainty in the velocity change of each object, we added it in quadrature with the uncertainty in aligning the SDSS and post-SDSS spectra via the [O III] lines (see the last paragraph of §5.1) to obtain the total uncertainty.

In Table 5 we summarize the results of theta cross-correlation analysis. In 14 cases the broad $H\beta$ peak velocities change significantly (at 99% confidence). In 38 cases we obtain only limits to possible shifts (at 99% confidence). In 10 of these cases we encountered small

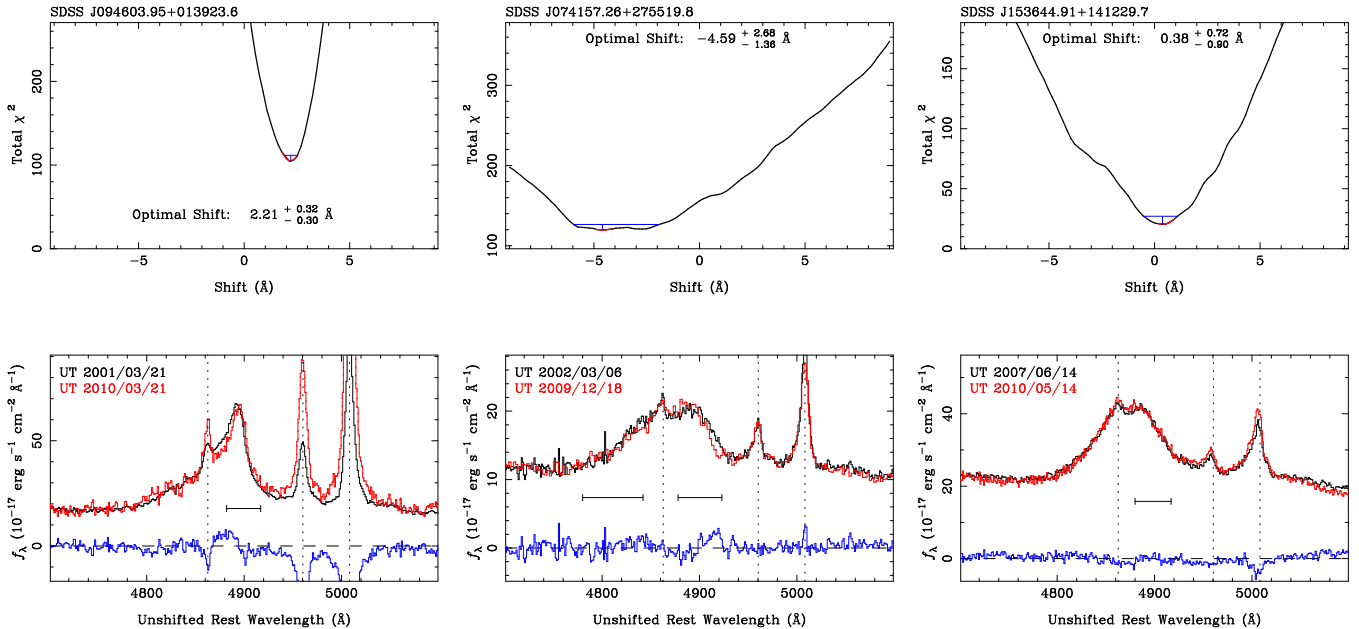


FIG. 9.— Examples of the application of our cross-correlation technique (see §6.1 of the text) to three pairs of spectra. In the lower panel of each set we show the two spectra appropriately scaled and superposed for comparison. The original SDSS spectrum (which is the one that is scaled, shifted and rebinned by the cross-correlation algorithm) is shown in red, while the residuals after subtraction of the two is shown in blue (in this illustration the residuals represent the difference between the *un-shifted* spectra). Since the scaling of the two spectra is such that the continuum and broad lines match, there is typically a mismatch between the narrow lines, which indicates that the continuum and/or the broad lines have varied between the two epochs. The vertical dotted lines mark the nominal positions of the narrow H β and [O III] lines. The horizontal error bars show the sections of the broad line profiles used by the cross-correlation algorithm. The upper panel of each set shows the variation of χ^2 with the shift applied to the post-SDSS (red) spectrum. The red arc at the trough of the χ^2 curve shows the global minimum and the (blue) horizontal line shows the 99% confidence level for one interesting parameter, $\chi_{\min}^2 + 6.63$. We note for reference that a wavelength shift of 1 \AA corresponds to a velocity shift of 62 km s^{-1} . The three examples shown here illustrate the following: *Left*: a significant shift of the offset peak of the broad line; *Middle*: a subtle profile variation that mimics a shift of the broad line in the χ^2 curve; *Right*: no significant shift of the offset peak.

TABLE 5
RESULTS OF CROSS-CORRELATION ANALYSIS

Object	Broad H β Shift ^a (km s^{-1})	Object	Broad H β Shift ^a (km s^{-1})	Object	Broad H β Shift ^a (km s^{-1})
J001224	$+125^{+35}_{-30}$	J102106	$[-250, +310]$	J141300	... ^d
J002444	$[-310, +110]$	J104132	... ^d	J143123	... ^b

The remaining objects have been omitted

^a Numbers with error bars denote a statistically significant shift. Pairs of numbers in square brackets denote upper and lower limits on the shift. A positive shift means that the post-SDSS spectrum is shifted towards longer wavelengths.

^b The broad H β profile varied substantially between observations, thus a meaningful shift could not be determined. These variations may include large changes in the profile shape or changes in the width that cause the two wings of the line to move in opposite directions.

^c Variability of the broad H β line profile affects our ability to determine a shift and increases the uncertainties.

^d The low S/N in the followup spectrum does not allow us to get meaningful constraints on the shift.

variations in the broad H β profiles, such as small changes in the widths or variations in one of the two wings. Even though we do report shifts or limits in these cases, they are subject to an additional systematic error, which we have included in the limits we report in Table 5. In the remaining 16 cases we are not able to obtain meaningful measurements of velocity changes, or limits, either because the broad H β profiles varied substantially between observations or because the S/N of one of the two spectra was extremely low. We also note that Shields et al. (2009b) have determined an upper limit to the velocity

change in J105041 of $31 \pm 60 \text{ km s}^{-1}$ (or $[-30, 90]$, in the notation of Table 5).

In Figure 10 we present our results graphically (including the limits on J105041, determined by Shields et al. 2009b). In the upper panel of this figure we plot the measured velocity change against the rest-frame time interval between observations. The statistically significant measurements are denoted by black, solid circles with 99%-confidence error bars, while 99%-confidence limits on the velocity changes are shown as grey error bars. An alternative representation of the results is shown in

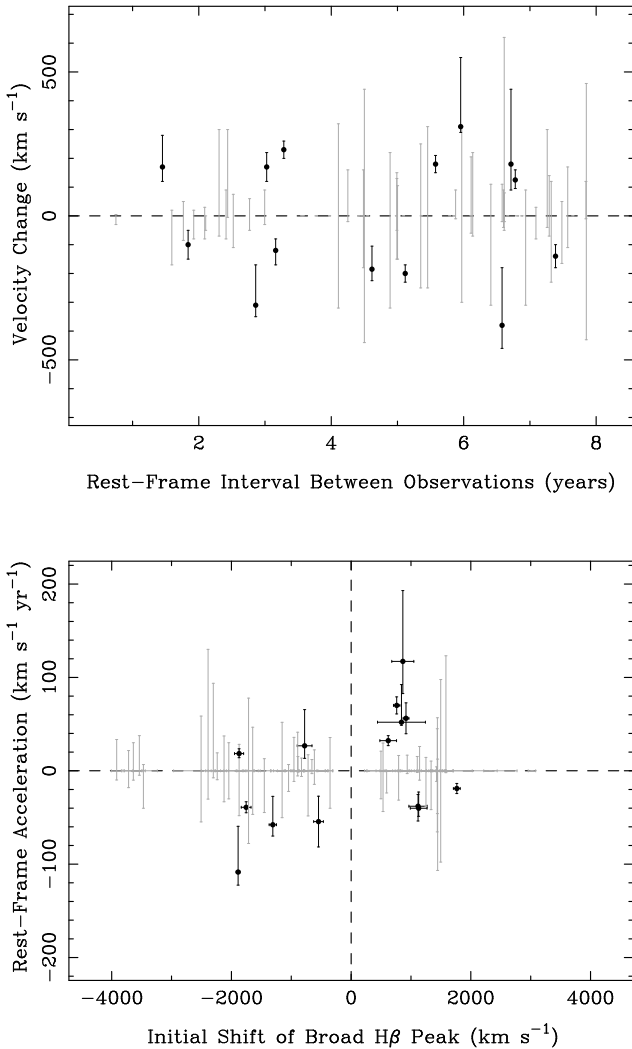


FIG. 10.— *Top*: Velocity change of broad $H\beta$ peak (Δv) plotted against the rest-frame time interval between observations. *Bottom*: Accelerations determined from changes in the broad $H\beta$ peak velocities ($\Delta v/\Delta t_{\text{rest}}$) plotted against the initial peak velocity (peak offset, as measured from the original SDSS spectra). In both panels, the black points with error bars show the objects where a significant change in the broad $H\beta$ peak velocity was measured in the time interval covered by the observations. The light grey error bars show objects where only upper limits on the velocity change were obtained (included are also the limits derived for J105041 by Shields et al. 2009b). All error bars and limits correspond to the 99% (2.6σ) confidence level.

the lower panel of the same figure where we plot the observed acceleration against the initial shift of the broad $H\beta$ peak (as measured from the SDSS spectra; see Table 4). We converted the velocity changes to accelerations ($\Delta v/\Delta t_{\text{rest}}$, in $\text{km s}^{-1} \text{ yr}^{-1}$) by dividing the velocity changes of Table 5 by the rest-frame time intervals between observations. The velocity changes appear to be distributed evenly with interval between observations. Moreover, there appears to be no relation between the acceleration and the initial velocity shift. We consider these findings further in our discussion of the results in §7.

6.3. Limitations and Caveats

As we noted above, there are a number of cases where the profile of the broad $H\beta$ line has varied substantially

between the SDSS and post-SDSS observations (see Table 5). Such an effect represents an inevitable limitation to our ability to determine changes in the velocity of the broad lines, which relies on the long-term stability of the profiles. Variability of the line profiles can occur on time scales comparable to the dynamical time of the BLR, which should be shorter than the orbital period of the hypothesized SBHB. Examples of objects with substantially variable broad $H\beta$ profile include J112751, J113706, J140700, and J180545 (see the comparison plots in Fig. 2). A particularly interesting example of substantial variability is J093653, where the broad $H\beta$ line declined in flux between the two epochs of observation with the result that the displaced peak of the broad line is now blended with the narrow line, making the measurement of a velocity change unreliable.

More subtle profile variations can also affect our ability to determine velocity changes. For example, in J074157 (see Fig. 9) the broad $H\beta$ line became narrower between the two observations and the line wings have moved closer to the line core, which prevents us from obtaining limits on the acceleration. In some cases, e.g., J091833, J111916, and J154340 (see Fig. 2), one of the two sides of the line has changed but the other has not; we can determine limits on the acceleration in such cases, but the uncertainties are larger than they would have been if the profile were stable, as we indicate in Table 5.

Yet another type of profile variability that can influence our results is a correlated change on the two sides of the broad $H\beta$ profile (a seesaw-like pattern) that can mimic a velocity change. Such variability cycles have been observed in broad double-peaked emission lines (see, for example, Lewis et al. 2010). The beginnings of this pattern are discernible in the spectra of J031715 and J160243 shown in Figure 2, for example. With this in mind, we note that some of the objects for which we report statistically significant velocity changes, specifically those where the shifted peak of the broad $H\beta$ line is partially blended with the narrow $H\beta$ line, may be subject to this effect (e.g., J093844, J120924). Thus, the velocity changes reported in Table 5 are subject to verification by future followup observations. There are, of course, additional reasons why further followup observations are needed, as we discuss in more detail in the next section.

7. DISCUSSION

7.1. Alternative Interpretations of Displaced Emission Line Peaks

Given that the starting point for our search for SBHBs and rapidly-recoiling BHs was the selection of broad Balmer lines whose peaks are displaced from their nominal wavelengths, additional observations are needed to find the strong candidates from the initial list. The reason is that we cannot exclude alternative interpretations for the displaced peaks of the broad lines such as an unusual structure or a perturbation of the BLR. For example, in the class of models where the BLR is the surface of the accretion disk or the base of the wind that is launched from it, perturbations in the form of large-scale spiral arms can create line profiles with a dominant peak or shoulder that is shifted from the nominal wavelength of the line. Examples of model profiles with such properties

can be found in Lewis et al. (2010, e.g., their Figure 36). In the same context, one can also envision cases where the broad Balmer lines from an unperturbed disk are double-peaked but a perturbation such as a spiral arm causes one of the two peaks to be considerably stronger than the other. Many examples of observed profiles that have such shapes can be found in the Appendix of Gezari et al. (2007); some of the more remarkable cases are reproduced in Figure 5 of Lauer & Boroson (2009). Therefore, it is essential to carry out monitoring observations to look for further variations in the velocities of the displaced peak of the broad line.

The detection of velocity changes in broad $H\beta$ lines between two epochs is only the first step in making the case that Balmer lines with displaced peaks are indeed signposts of SBHBs. Many monitoring observations are needed to verify that the velocity changes continue monotonically and that they follow the pattern expected for orbital motion. In particular the peaks of the broad line must drift from a negative velocity to a positive velocity and *vice versa*. Since our understanding of the structure and dynamics of the gas in the BLR is incomplete, we cannot select SBHBs without observing complete orbital cycles because intrinsic variations of the broad line profiles on time scales of several years may resemble the pattern of orbital motion. A good case in point is provided by Mrk 668 (included in our sample here as J140700). This object was one of the first two proposed SBHBs (Gaskell 1983) and the variability of its broad Balmer lines has been monitored over a long period of time (~ 16 years; see Marziani et al. 1993; Gezari et al. 2007). Although the velocity of the peak of the Balmer lines does change sign, the radial velocity curve is not compatible with orbital motion: the shape of the curve is not sinusoidal, the wings of the line profile do not change accordingly (see Figures 30 and 31 of Gezari et al. 2007), and the center of mass of a hypothesized binary appears to be at a different velocity than the host galaxy (Marziani et al. 1993). This point is also bolstered by the case of 3C 390.3, a double-peaked emitter whose $H\beta$ line changed in a manner reminiscent of orbital motion by $\sim \frac{1}{4}$ of a cycle (Gaskell 1996). The pattern changed drastically however after that and became incompatible with orbital motion (Eracleous et al. 1997; Shapovalova et al. 2001). More examples of broad Balmer lines with displaced peaks whose velocities have varied in a manner inconsistent with orbital motion can be found in Gezari et al. (2007) and Lewis et al. (2010). The need for long-term monitoring makes the search for SBHBs a challenging exercise in patience and persistence since the expected orbital periods can be quite long (see equation [4] and the associated discussion).

Notwithstanding the caveats listed above, we consider the consequences of our findings for the two scenarios we have set out to test. In summary, the main observational results of this work that bear directly on our tests are: (a) We have identified 88 quasars at $z \lesssim 0.7$ (among 15,900 quasars from SDSS DR7) whose broad $H\beta$ lines are shifted from their nominal positions by a few $\times 1,000$ km s^{-1} , (b) we have measured statistically significant accelerations of the offset peaks (in the range of -120 to $+120$ km s^{-1} yr $^{-1}$) in 14/68 objects via followup observations, (c) we have measured the properties

of the broad $H\beta$ lines from the SDSS spectra and found a correlation between the skewness of the profiles and the velocity offset of the peak, which suggests that all the objects of this sample belong to the same family, i.e., have a single, common physical explanation and (d) we have measured the properties several narrow, forbidden, optical emission lines and found them to be very similar to those of typical quasars.

7.2. Implications for Rapidly Recoiling BHs

The rapidly recoiling BH hypothesis, remains a viable possibility for objects in this sample. This is because the primary observable, the velocity offset of the broad emission lines, can be interpreted both as a result of an SBHB and as a result of a large recoil speed. Observational tests that have been proposed to distinguish between the two interpretations are indirect. The likelihood that a significant fraction of our sample are rapidly recoiling black holes appears low a priori on theoretical grounds. In particular, Dotti et al. (2010) find that only 0.2% of all recoil speeds should exceed 400 km s^{-1} , while the distribution of line shifts that we find, if all of these are interpreted as recoil speeds, implies that $> 0.5\%$ of recoil speeds exceed 1,000 km s^{-1} . In the cases where we were able to measure an acceleration, a rapidly recoiling BH interpretation is not ruled out because intrinsic variability of the line profiles can mimic an acceleration as we discuss in §7.1. However, if the accelerations we have measured are confirmed to be real accelerations, that would weaken the case for a rapidly recoiling BH and strengthen the SBHB interpretation for those particular objects.

An observational selection criterion for recoiling BH candidates, proposed by Bonning et al. (2007), is based on the widths of the narrow, forbidden lines. If the displaced quasar is illuminating the gas in its former host galaxy from the outside, the narrow-line region is not stratified in ionization, thus the widths of all the narrow, forbidden lines should be approximately the same. If, however, the gas emitting the narrow lines is associated with the recoiling BH (it could originate, for example, from biconical outflows from the accretion disk, as suggested by Komossa et al. 2008), the widths of the lines would not be a good indicator of such a system since they may display all the trends observed in Seyfert galaxies. In such a case the luminosities and relative intensities of the narrow emission lines may provide a better test for recoiling BHs than their widths.

Nevertheless, in the 50 quasars for which we were able to measure the FWHM of the [Ne V], [Ne III], and [O III] lines, there are 9 cases where the widths of these lines appear to be the same within 10%. In 8 of these cases, the [O II] lines are significantly narrower. The exception is J084313, where the width of the [O II] is comparable to that of the other forbidden lines. In this object, the velocity offset of the broad $H\beta$ line from the system of the narrow lines is only -610 km s^{-1} and the profile of the line is fairly symmetric, as indicated by the skewness coefficients (this is another important consideration for selecting candidate recoiling BHs according to Shields et al. 2009b). In spite of the above, the relative strengths of the narrow, forbidden lines of this object are very typical of a Seyfert galaxy, which suggests that the ionization parameter of the gas in the narrow-line region should be similar to that of Seyferts. This is not

in agreement with the proposed picture of a displaced quasar that illuminates its host galaxy from a significant distance. The quasar J092712, proposed as a candidate rapidly recoiling BH by Komossa et al. (2008), has two systems of narrow lines and in the one that would be attributed to the (former) host galaxy in this interpretation the narrow lines are unusually narrow and have similar widths. However, alternative interpretations have also been proposed (Bogdanović et al. 2009; Dotti et al. 2009a; Shields et al. 2009a; Heckman et al. 2009), which means that the rapidly recoiling BH scenario is not a unique interpretation for this very unusual object.

We note in conclusion that the process of photoionization of the gas in a galaxy by an offset or neighboring AGN warrants further investigation in order to develop more quantitative and robust emission-line diagnostics. On the theoretical side, the photoionization calculations of Gnedin (1997) can be extended to cover a wider range of conditions and to make predictions for the relative intensities, luminosities, and profiles of the narrow emission lines. On the observational side, progress can be made by seeking out and studying more analogs of the Was 49 system (Moran et al. 1992), a dual Seyfert galaxy in which the more luminous AGN contributes to the ionization of the interstellar medium of the host galaxy of its less luminous neighbor.

7.3. Implications for SBHBs

Considering our results in the context of the SBHB hypothesis, we can compare them with the specific predictions made by Volonteri et al. (2009) for the number of such systems that may be present in the SDSS DR7 quasar sample at $z < 0.7$. If we suppose that all of the objects in our sample are SBHBs, then their number is broadly consistent with one of the two models considered by Volonteri et al. (2009), their model I. According to this model, which is based on the assumption that all SBHBs are active (i.e., accreting) regardless of the merger history of their host, there are at most 160 systems with $q > 10^{-2}$ in the SDSS DR7 quasar sample. If we only take the 14 systems with detectable velocity changes to be SBHBs, their number is broadly consistent with model II of Volonteri et al. (2009) according to which SBHBs are active only in the aftermath of a major merger. Under the assumptions of this model the predicted number of SBHBs with $q > 10^{-2}$ in the SDSS DR7 quasar sample is 16. The comparison of the above predictions with the observational results is complicated by a number of uncertainties. On the theoretical side: (a) the models refer to a volume-limited sample of quasars, while the SDSS quasar sample is not volume limited (given the flux limit of the quasar catalog, quasars with i magnitudes between 19.1 and 21.2 are missed even though they would satisfy the quasar luminosity criterion), (b) the predicted numbers quoted above rely on the assumption that both of the BHs in a binary may accrete (with an assumed distribution of Eddington ratios), without regard to their relative luminosity, while our selection method picks out systems in which the BLR around only one of the two BHs is visible, (c) inclusion in the theoretical sample is based on the luminosity of the primary, regardless of whether or not it is less luminous than the secondary. The above uncertainties can change the upper limits quoted above in either direction.

On the observational side: (a) some of the candidates we report may turn out not to be SBHBs for the reasons discussed in §7.1, (b) if we assume that our selection method is appropriate for finding SBHBs, we are likely to have missed systems with small projected orbital velocities (i.e., systems viewed close to face on, or caught near conjunction, or with a combination of low masses and wide separations), and (c) the number of objects for which a measurable acceleration is likely to change with future observations.

Assuming that velocity changes we have measured correspond to orbital accelerations in an SBHB we can explore the implications of the results for this hypothesis. The correlation between the skewness of the broad $H\beta$ profiles and the shift of their peaks (see Figure 5) suggests that all the objects in this sample belong to the same family¹², therefore we ask why an acceleration was measurable only in a small fraction of the sample. As we noted in §2 we expect that the SBHBs we can detect with our strategy can have periods from a few decades to a few centuries depending on the total mass of the binary and the observed velocity shift, which constrains the orbital separation given the masses of the two BHs. As pointed out by Loeb (2010), the likelihood of finding a system with a given set of intrinsic properties depends on its decay time via emission of gravitational radiation. This can be estimated from the formula of Peters (1964), which we can cast in terms of intrinsic system properties and observables using equation (4) as follows:

$$\begin{aligned} t_{\text{gr}} &= \frac{5}{256} \frac{c^5 a^4}{(GM)^3} \frac{(1+q)^2}{q} \\ &= 4 \times 10^{13} M_8 \frac{(1+q)^2}{q} \left[\frac{\sin i |\sin \phi|}{(1+q) u_{2,3}} \right]^8 \text{ yr} \quad (7) \\ &= \frac{8 \times 10^{11} M_8}{(1+q)^6 u_{2,3}^8} \left(\frac{0.1}{q} \right) \left[\frac{\sin i}{\sin 45^\circ} \frac{|\sin \phi|}{\sin 45^\circ} \right]^8 \text{ yr}. \end{aligned}$$

Since the lifetime of an observed SBHB is such a sensitive function of the observed velocity offset of the broad emission line, $u_{2,3}$, we would expect that low-mass, high-speed binaries should be extremely rare since their orbits should be rapidly decaying by gravitational radiation. Specifically, setting $M_8 = 0.1$ and $u_{2,3} = 2$ in equation (7) gives $t_{\text{gr}} \approx 3 \times 10^8$ yr, while setting $M_8 = 1$ and $u_{2,3} = 3$ gives $t_{\text{gr}} \approx 1 \times 10^8$ yr. The above considerations lead us to conclude that systems with observed velocity shifts in excess of $1,000 \text{ km s}^{-1}$ may be (a) highly inclined (hence with large separations, according to equation [4]), (b) caught near quadrature, (c) very massive, or (d) very small mass-ratio systems ($q \ll 0.1$). Under different conditions, such systems would have very short lifetimes. The relatively uniform distribution of velocity changes and accelerations depicted in Figure 10 suggests that a combination of the above four effects is at work. Highly inclined or massive systems would have low accelerations, according to equation (5), which may explain why we were not able to detect an acceleration in the majority of the objects we have followed up. Continued

¹² This is an optimistic hypothesis. A more pessimistic interpretation of this correlation is, of course, that none of the objects in our sample are SBHBs.

monitoring can discriminate among the above possibilities by providing constraints on the binary phase through the shape of the radial velocity curve.

Useful constraints on the properties of a hypothesized SBHB can be obtained from a few observations spanning a baseline of about a decade. Accurate measurements of the velocities of the peaks over such a baseline can constrain the curvature of the radial velocity curve and yield a lower limit on the period and total mass of the SBHB. This technique, pioneered by Halpern & Filippenko (1988) and developed further by Eracleous et al. (1997), was used to test and eventually reject the SBHB hypothesis for three quasars with double-peaked Balmer lines. An application of the same technique to objects from the present sample can lead to similar constraints, which could render the SBHB hypothesis untenable if these constraints are restrictive enough. To this end, we are continuing to monitor all of our targets with the immediate goal of collecting a few radial velocity measurements for each object and using them to evaluate the plausibility of the SBHB hypothesis by the above method.

Another avenue for testing the SBHB hypothesis for shifted broad Balmer line peaks involves a comparison of the profiles of the Ly α and Balmer lines. If the displaced peaks originate in a perturbed disk around a single BH rather than in a BLR bound to one of the two BHs in SBHB, we would expect the profiles of the broad optical and UV emission lines to differ considerably. This expectation is based on an analogy with nearby, well-studied double-peaked emitters (see, for ex-

ample, Eracleous 2006; Eracleous et al. 2009). The most dramatic difference in such a case is between the profile of Ly α , which peaks at its nominal wavelength and those of the Balmer lines whose peaks are displaced. We are currently pursuing this test using UV spectra from the *Hubble Space Telescope*.

We are grateful to Steinn Sigurdsson for many stimulating discussions and to Tamara Bogdanović for her critical reading of the manuscript. We also acknowledge helpful discussions with Marta Volonteri and Cole Miller. M.E. gratefully acknowledges the hospitality of the Aspen Center for Physics where the final stages of this work were carried out.

The Hobby-Eberly Telescope (HET) is a joint project of the University of Texas at Austin, the Pennsylvania State University, Stanford University, Ludwig-Maximilians-Universität München, and Georg-August-Universität Göttingen. The HET is named in honor of its principal benefactors, William P. Hobby and Robert E. Eberly.

The Marcario Low-Resolution Spectrograph is named for Mike Marcario of High Lonesome Optics, who fabricated several optics for the instrument but died before its completion; it is a joint project of the Hobby-Eberly Telescope partnership and the Instituto de Astronomía de la Universidad Nacional Autónoma de México.

This research has made use of the NASA/IPAC Extragalactic Database (NED) which is operated by the Jet Propulsion Laboratory, California Institute of Technology, under contract with the National Aeronautics and Space Administration.

REFERENCES

- Armitage, P. J. & Natarajan, P. 2005, *ApJ*, 634, 921
 Artymowicz, P., Clarke, C. J., Lubow, S. H., & Pringle, J. E. 1991, *ApJ*, 370, L35
 Artymowicz, P. & Lubow, S. H. 1996, *ApJ*, 467, L77
 Baker, J. G., Boggs, W. D., Centrella, J., Kelly, B. J., McWilliams, S. T., Miller, M. C., & Van Meter, J. R. 2008, *ApJ*, 682, L29
 Barrows, R. S., Lacy, C. H. S., Kenefick, D., Kenefick, J., & Seigar, M. S. 2011, *New Astr.*, 16, 122
 Begelman, M. C., Blandford, R. D., & Rees, M. J. 1980, *Nature*, 287, 307
 Berczik, P., Merritt, D., Spurzem, R., & Bischof, H.-P. 2006, *ApJ*, 642, L21
 Bernardi, M. et al. 2003, *AJ*, 125, 1817
 Blecha, L., Cox, T. J., Loeb, A., & Hernquist, L. 2010, *MNRAS*, 412, 2154
 Bogdanović, T., Reynolds, C. S., & Miller, M. C. 2007, *ApJ*, 661, L147
 Bogdanović, T., Smith, B. D., Sigurdsson, S., & Eracleous, M. 2008, *ApJS*, 174, 455
 Bogdanović, T., Eracleous, M., & Sigurdsson, S. 2009, *ApJ*, 697, 288
 Bonning, E. W., Shields, G. A., & Salvander, S. 2007, *ApJ*, 666, L13
 Boroson, T. A. & Lauer, T. R. 2009, *Nature*, 458, 53
 Boroson, T. A. & Lauer, T. R. 2010, *AJ*, 140, 390
 Boroson, T. A. & Green, R. F. 1992, *ApJS*, 80, 109
 Campanelli, M., Lousto, C., Zlochower, Y., & Merritt, D. 2007, *ApJ*, 659, L5
 Campanelli, M., Lousto, C. O., Zlochower, Y., & Merritt, D. 2007, *Phys. Rev. Lett.*, 98, 231102
 Centrella, J., Baker, J. G., Kelly, B. J., & Van Meter, J. R. 2010, *Reviews of Modern Physics*, 82, 3069
 Centrella, J., Baker, J. G., Kelly, B. J., & Van Meter, J. R. 2010, *Annual Review of Nuclear and Particle Science*, 60, 75
 Chen, K., Halpern, J. P., & Filippenko, A. V. 1989, *ApJ*, 339, 742
 Chang, P., Strubbe, L. E., Menou, K., & Quataert, E. 2010, *MNRAS*, 407, 2007
 Chornock, R., et al. 2010, *ApJ*, 709, L39
 Civano, F. et al. 2010, *ApJ*, 717, 209
 Comerford, J. M., et al. 2009a, *ApJ*, 698, 956
 Comerford, J. M., Griffith, R. L., Gerke, B. F., Cooper, M. C., Newman, J. A., Davis, M., & Stern, D. 2009b, *ApJ*, 702, L82
 Crenshaw, D. M., Schmitt, H. R., Kraemer, S. B., Mushotzky, R. F., & Dunn, J. P. 2010, *ApJ*, 708, 419
 Cuadra, J., Armitage, P. J., Alexander, R. D., & Begelman, M. C. 2009, *MNRAS*, 393, 1423
 Decarli, R., Dotti, M., Montuori, C., Liimets, T., & Ederoclite, A. 2010, *ApJ*, 720, L93
 Di Matteo, T., Springel, V., & Hernquist, L. 2005, *Nature*, 433, 604
 Dotti, M., Colpi, M., Haardt, F., & Mayer, L. 2007, *MNRAS*, 379, 956
 Dotti, M., Montuori, C., Decarli, R., Volonteri, M., Colpi, M., & Haardt, F. 2009, *MNRAS*, 398, L73
 Dotti, M., Ruzzkowski, M., Paredi, L., Colpi, M., Volonteri, M., & Haardt, F. 2009, *MNRAS*, 396, 1640
 Dotti, M., Volonteri, M., Perego, A., Colpi, M., Ruzzkowski, M., & Haardt, F. 2010, *MNRAS*, 402, 682
 Eracleous, M., Livio, M., Halpern, J. P., & Storchi-Bergmann, T. 1995, *ApJ*, 438, 610
 Eracleous, M., Halpern, J. P., Gilbert, A. M., Newman, J. A., & Filippenko, A. V. 1997, *ApJ*, 490, 216
 Eracleous, M. & Halpern, J. P. 2003, *ApJ*, 599, 886
 Eracleous, M. 2006, in *AGN Variability from the X-Rays to the Radio*, eds. C. M. Gaskell et al., ASP Conf. Ser. 360, 217
 Eracleous, M., Lewis, K. T., & Flohic, H. M. L. G. 2009, *New Ast. Rev.* 53, 133
 Escala, A., Larson, R. B., Coppi, P. S., & Mardones, D. 2004, *ApJ*, 607, 765
 Ferrarese, L. & Merritt, D. 2000, *ApJ*, 539, L9

- Filippenko, A. V. & Halpern, J. P. 1984, *ApJ*, 285, 458
- Fu, H., Myers, A. D., Djorgovski, S. G., & Yan, L. 2010, *ApJ* (Letters), submitted (arXiv:1009.0767)
- Gaskell, C. M. 1983, in *Quasars and Gravitational Lenses*, ed. J.-P. Swings, Liège International Astrophysical Colloquium (Liège: Université de Liège), 24, 473
- Gaskell, C. M. 1984, *Annals of the New York Academy of Sciences*, 422, 349
- Gaskell, C. M. 1996, *ApJ*, 464, L107
- Gaskell, C. M. 2010, *Nature*, 463, E1
- Gezari, S., Halpern, J. P., & Eracleous, M. 2007, *ApJS*, 169, 167
- Gebhardt, K., et al. 2000, *ApJ*, 539, L13
- Gnedin, O. Y. 1997, *ApJ*, 491, 69
- Gopal-Krishna, Biermann, P. L., & Wiita, P. J. 2003, *ApJ*, 594, L103
- Gould, A. & Rix, H.-W. 2000, *ApJ*, 532, L29
- Gualandris, A. & Merritt, D. 2008, *ApJ*, 678, 780
- Halpern, J. P. & Filippenko, A. V. 1988, *Nature*, 331, 46
- Hayasaki, K., Mineshige, S., & Sudou, H. 2007, *PASJ*, 59, 427
- Heckman, T. M., Krolik, J. H., Moran, S. M., Schnittman, J., & Gezari, S. 2009, *ApJ*, 695, 363
- Hogg, D. 1999, arXiv:astro-ph/9905116
- Hopkins, P. F., Hernquist, L., Cox, T. J., Di Matteo, T., Robertson, B., & Springel, V. 2006, *ApJS*, 163, 1
- Jester, S. et al. 2005, *AJ*, 130, 873
- Komberg, B. V. 1968, *Sov. Astr.*, 11, 727
- Komossa, S., Burwitz, V., Hasinger, G., Predehl, P., Kaastra, J. S., & Ikebe, Y. 2003, *ApJ*, 582, L15
- Komossa, S., Zhou, H., & Lu, H. 2008, *ApJ*, 678, L81
- Komossa, S. & Merritt, D. 2008, *ApJ*, 689, L89
- Lampton, M., Margon, B., & Bowyer, S. 1976, *ApJ*, 208, 177
- Laor, A., Barth, A. J., Ho, L. C., & Filippenko, A. V. 2006, *ApJ*, 636, 83
- Lauer, T. R. & Boroson, T. A. 2009, *ApJ*, 703, 930
- Lewis, K. T., Eracleous, M., & Storchi-Bergmann, T. 2010, *ApJS*, 187, 416
- Liu, X., Shen, Y., Strauss, M. A., & Greene, J. E. 2010a, *ApJ*, 708, 427
- Liu, X., Greene, J. E., Shen, Y., & Strauss, M. A. 2010b, *ApJ*, 715, L30
- Lodato, G., Nayakshin, S., King, A. R., & Pringle, J. E. 2009, *MNRAS*, 398, 1392
- Loeb, A. 2007, *Phys. Rev. Lett.*, 99, 041103
- Loeb, A. 2010, *Phys. Rev. D*, 81, 047503
- Maness, H. L., Taylor, G. B., Zavala, R. T., Peck, A. B., & Pollack, L. K. 2004, *ApJ*, 602, 123
- Marziani, P., Sulentic, J. W., Calvani, M., Perez, E., Moles, M., & Penston, M. V. 1993, *ApJ*, 410, 56
- Mathews, W. G. & Capriotti, E. R. 1985, in *Astrophysics of Active Galaxies and Quasi-Stellar Objects*, ed J. S. Miller (Mill Valley: University Science Books), 185
- Milosavljević, M., Merritt, D., Rest, A., & Van Den Bosch, F. C. 2002, *MNRAS*, 331, L51
- Milosavljević, M. & Merritt, D. 2003, *ApJ*, 596, 860
- Merritt, D. & Ekers, R. D. 2002, *Science*, 297, 1310
- Merritt, D. 2006, *ApJ*, 648, 976
- Montuori, C., Dotti, M., Colpi, M., Decarli, R., & Haardt, F. 2010, *MNRAS*, submitted (arXiv:1010.4303)
- Moore, D., Cohen, R. D., & Marcy, G. W. 1996, *ApJ*, 470, 280
- Morton D. C. 1991, *ApJS*, 77, 119
- Moran E. C., Halpern, J. P., Bothun, G. D., & Becker, R. H. 1991, *AJ*, 104, 990
- Nagao, T., Murayama, T., & Taniguchi, Y. 2001, *PASJ*, 53, 629
- Peters, P. 1964, *Phys. Rev.*, 136, 1224
- Peterson, B. M., Korista, K. T., & Cota, S. A. 1987, *ApJ*, 312, L1
- Peterson, B. M., et al. 2002, *ApJ*, 581, 197
- Rödig, C., Dotti, M., Sesana, A., Cuadra, J. & Colpi, M. 2011, *MNRAS*, submitted (arXiv:1104.3868)
- Rodriguez, C., Taylor, G. B., Zavala, R. T., Peck, A. B., Pollack, L. K., & Romani, R. W. 2006, *ApJ*, 646, 49
- Rodriguez, C., Taylor, G. B., Zavala, R. T., Pihlström, Y. M., & Peck, A. B. 2009, *ApJ*, 697, 37
- Romero, G. E., Chajet, L., Abraham, Z., & Fan, J. H. 2000, *A&A*, 360, 57
- Roos, N., Kaastra, J. S., & Hummel, C. A. 1993, *ApJ*, 409, 130
- Salviander, S., Shields, G. A., Gebhardt, K., & Bonning, E. W. 2007, *ApJ*, 662, 131
- Schlegel, D. J., Finkbeiner, D. P. & Davis, M. 1998, *ApJ*, 500, 525
- Schneider, D. P. et al. 2010, *AJ*, 139, 2360
- Seaton, M. J. 1979, *MNRAS*, 187, 83P
- Sergeev, S. G., Doroshenko, V. T., Dzyuba, S. A., Peterson, B. M., Pogge, R. W., & Pronik, V. I. 2007, *ApJ*, 668, 708
- Sesana, A., Haardt, F., Madau, P., & Volonteri, M. 2005, *ApJ*, 623, 23
- Sesana, A., Haardt, F., & Madau, P. 2007, *ApJ*, 660, 546
- Shapovalova, A. I., et al. 2001, *A&A*, 376, 775
- Shen, Y. & Loeb, A. 2010a, *ApJ*, 725, 249
- Shen, Y., Liu, X., Greene, J., & Strauss, M. 2010b, arXiv:1011.5246
- Shields, G. A., Bonning, E. W., & Salviander, S. 2009a, *ApJ*, 696, 1367
- Shields, G. A., et al. 2009b, *ApJ*, 707, 936
- Smith, K., et al. 2010a, *BAAS*, 42, 371
- Smith, K. L., Shields, G. A., Bonning, E. W., McMullen, C. C., Rosario, D. J., & Salviander, S. 2010b, *ApJ*, 716, 866
- Stirpe, G. M. 1990, *A&AS*, 85, 1049
- Strateva, I. V., et al. 2003, *AJ*, 126, 1720
- Sulentic, J. W., Marziani, P., Zamanov, R., Bachev, R., Calvani, M., & Dultzin-Hacyan, D. 2002, *ApJ*, 566, L71
- Tang, S. & Grindlay, J. 2009, *ApJ*, 704, 1189
- Tsalamantza, P., Decarli, R., Dotti, M., & Hogg, D. W. 2011, *ApJ*, in press (arXiv:1106.1180v1)
- Valtonen, M. J., et al. 2008, *Nature*, 452, 851
- Vanden Berk, D. E. et al. 2001, *AJ*, 122, 549
- Volonteri, M., Haardt, F., & Madau, P. 2003, *ApJ*, 582, 559
- Volonteri, M., Miller, J. M., & Dotti, M. 2009, *ApJ*, 703, L86
- Volonteri, M., Gültekin, K., & Dotti, M. 2010, *MNRAS*, 404, 2143
- Wanders, I. & Peterson, B. M. 1996, *ApJ*, 466, 174
- Whittle, M. 1985, *MNRAS*, 216, 817
- Zamfir, S., Sulentic, J. W., Marziani, P., & Dultzin, D. 2010, *MNRAS*, 403, 1759